Multimodel projections of stratospheric ozone in the 21st century

V. Eyring,[1] D. W. Waugh,[2] G. E. Bodeker,[3] E. Cordero,[4] H. Akiyoshi,[5] J. Austin,[6] S. R. Beagley,[7] B. A. Boville,[8] P. Braesicke,[9] C. Brühl,[10] N. Butchart,[11] M. P. Chipperfield,[12] M. Dameris,[1] R. Deckert,[1] M. Deushi,[13] S. M. Frith,[14] R. R. Garcia,[8] A. Gettelman,[8] M. A. Giorgetta,[15] D. E. Kinnison,[8] E. Mancini,[16] E. Manzini,[17] D. R. Marsh,[8] S. Matthes,[1] T. Nagashima,[5] P. A. Newman,[18] J. E. Nielsen,[14] S. Pawson,[18] G. Pitari,[16] D. A. Plummer,[19] E. Rozanov,[20] M. Schraner,[21] J. F. Scinocca,[22] K. Semeniuk,[7] T. G. Shepherd,[23] K. Shibata,[13] B. Steil,[10] R. S. Stolarski,[18] W. Tian,[12] and M. Yoshiki[5]

Received 11 December 2006; revised 18 May 2007; accepted 30 May 2007; published 21 August 2007.

[1] Simulations from eleven coupled chemistry-climate models (CCMs) employing nearly identical forcings have been used to project the evolution of stratospheric ozone throughout the 21st century. The model-to-model agreement in projected temperature trends is good, and all CCMs predict continued, global mean cooling of the stratosphere over the next 5 decades, increasing from around 0.25 K/decade at 50 hPa to around 1 K/decade at 1 hPa under the Intergovernmental Panel on Climate Change (IPCC) Special Report on Emissions Scenarios (SRES) A1B scenario. In general, the simulated ozone evolution is mainly determined by decreases in halogen concentrations and continued cooling of the global stratosphere due to increases in greenhouse gases (GHGs). Column ozone is projected to increase as stratospheric halogen concentrations return to 1980s levels. Because of ozone increases in the middle and upper stratosphere due to GHG-induced cooling, total ozone averaged over midlatitudes, outside the polar regions, and globally, is projected to increase to 1980 values between 2035 and 2050 and before lower-stratospheric halogen amounts decrease to 1980 values. In the polar regions the CCMs simulate small temperature trends in the first and second half of the 21st century in midwinter. Differences in stratospheric inorganic chlorine (Cl_y) among the CCMs are key to diagnosing the intermodel differences in simulated ozone recovery, in particular in the Antarctic. It is found that there are substantial quantitative differences in the simulated Cl_y, with the October mean Antarctic Cl_y peak value varying from less than 2 ppb to over 3.5 ppb in the CCMs, and the date at which the Cl_y returns to 1980 values varying from before 2030 to after 2050. There is a similar variation in the timing of recovery of Antarctic springtime column ozone back to 1980 values. As most models underestimate peak Cl_y near 2000, ozone recovery in the Antarctic could occur even later, between 2060 and 2070. In the Arctic the column ozone increase in spring does not follow halogen decreases as closely as in the Antarctic, reaching 1980 values before Arctic halogen amounts decrease

[1]Institut für Physik der Atmosphäre, Deutsches Zentrum für Luft- und Raumfahrt, Oberpfaffenhofen, Germany.
[2]Department of Earth and Planetary Sciences, Johns Hopkins University, Baltimore, Maryland, USA.
[3]National Institute of Water and Atmospheric Research, Lauder, New Zealand.
[4]Department of Meteorology, San Jose State University, San Jose, California, USA.
[5]National Institute for Environmental Studies, Tsukuba, Japan.
[6]Geophysical Fluid Dynamics Laboratory, NOAA, Princeton, New Jersey, USA.
[7]Department of Earth and Space Science and Engineering, York University, Toronto, Ontario, Canada.
[8]National Center for Atmospheric Research, Boulder, Colorado, USA.
[9]Centre for Atmospheric Science, Cambridge University, Cambridge, UK.
[10]Max-Planck-Institut für Chemie, Mainz, Germany.
[11]Met Office Climate Research Division, Exeter, UK.
[12]Institute for Atmospheric Science, University of Leeds, Leeds, UK.
[13]Meteorological Research Institute, Tsukuba, Japan.
[14]Science Systems and Applications, Incorporated, Lanham, Maryland, USA.
[15]Max-Planck-Institut für Meteorologie, Hamburg, Germany.
[16]Università L'Aquila, Dipartimento di Fisica, L'Aquila, Italy.
[17]Istituto Nazionale di Geofisica e Vulcanologia and Centro Euro-Mediterraneo per i Cambiamenti Climatici, Bologna, Italy.
[18]NASA Goddard Space Flight Center, Greenbelt, Maryland, USA.
[19]Environment Canada, Toronto, Ontario, Canada.
[20]Institute for Atmospheric and Climate Science ETHZ and Physical-Meteorological Observatory, Davos, World Radiation Center, Switzerland.
[21]Institute for Atmospheric and Climate Science, ETH Zurich, Switzerland.
[22]Canadian Centre for Climate Modelling and Analysis, Meteorological Service of Canada, University of Victoria, Victoria, British Columbia, Canada.
[23]Department of Physics, University of Toronto, Toronto, Ontario, Canada.

Copyright 2007 by the American Geophysical Union.
0148-0227/07/2006JD008332

to 1980 values and before the Antarctic. None of the CCMs predict future large decreases in the Arctic column ozone. By 2100, total column ozone is projected to be substantially above 1980 values in all regions except in the tropics.

Citation: Eyring, V., et al. (2007), Multimodel projections of stratospheric ozone in the 21st century, *J. Geophys. Res.*, *112*, D16303, doi:10.1029/2006JD008332.

1. Introduction

[2] The stratospheric ozone layer has been depleted by anthropogenic emissions of halogenated species since the 1980s. Observations show that tropospheric halogen loading is now decreasing [*Montzka et al.*, 2003], which reflects the controls of ozone-depleting substances (ODSs) by the Montreal Protocol and its Amendments and Adjustments. Ozone is expected to continue to respond to these changes in ODSs but the timing and sensitivity of the response will depend on other changes in the atmosphere. Atmospheric concentrations of greenhouse gases (GHGs) have also increased and are expected to further increase in the future [*IPCC*, 2000] with consequences for the ozone layer. As a result of climate change, it is unlikely that the ozone layer will return to precisely its pre-1980 unperturbed state when the abundance of halogens returns to background levels. Furthermore, climate change complicates the attribution of ozone recovery to the decline of halogenated species.

[3] For these reasons, there is considerable interest in the interaction between ozone recovery and climate change through the rest of this century. To predict the future evolution of stratospheric ozone and attribute its behavior to the different forcings, models are required that can adequately represent both the chemistry of the ozone layer and the dynamics and energetics of the atmosphere, as well as their natural variability. Such models, known as coupled chemistry-climate models (CCMs), are three-dimensional atmospheric circulation models with fully coupled chemistry, i.e., where chemical reactions drive changes in atmospheric composition which in turn change the atmospheric radiative balance and hence dynamics. While the first CCMs were introduced approximately 15 years ago, it is only in the last decade that they have emerged as tools for making ozone climate projections [*Austin et al.*, 2003; *WMO/UNEP*, 2003, 2007].

[4] In support of the 2006 WMO/UNEP Scientific Assessment of Ozone Depletion [*WMO/UNEP*, 2007, chapter 6], the Chemistry-Climate Model Validation activity (CCMVal) for Stratospheric Processes and their Role in Climate (SPARC) project [*Eyring et al.*, 2005a, 2005b] proposed reference simulations for the past and for the future, to encourage consistency of anthropogenic and natural forcings as well as experimental set up in the CCM simulations. Confidence in CCM projections of future changes in atmospheric composition can be gained by first ensuring that the CCMs are able to reproduce past observations. Limitations and deficiencies in the models can be revealed through intermodel comparisons and through comparisons with observations. *Eyring et al.* [2006] evaluated simulations of the past from the current generation of thirteen CCMs. The primary objective of this paper is to examine the multimodel projections of stratospheric ozone in the 21st century from the same CCMs. The focus is on decadal ozone changes in three phases: (1) at the beginning of the century (2000–2020), (2) around midcentury (2040–2050 in extrapolar regions, 2060–2070 in polar regions), and (3) toward the end of the century (2090–2100). At the beginning of the century stratospheric halogen loading is expected to start to decrease or continue to decrease, around midcentury stratospheric halogen loading is expected to fall below 1980 values, and by the end of the century factors other than ODSs are expected to control stratospheric ozone [*IPCC/TEAP*, 2005].

[5] The models and simulations used in this study are described in section 2. Before examining the evolution of ozone in the models we investigate in section 3 projected future changes in stratospheric halogens, temperature and water vapor, and briefly discuss how dynamical changes and changes in total reactive nitrogen (NO_y) could alter the evolution of ozone. The multimodel projections of stratospheric ozone in the midlatitudes, tropics and polar regions for the 21st century are examined in section 4. Section 5 closes with a summary and conclusions.

2. Models and Model Simulations

[6] Simulations from eleven CCMs are used to predict the evolution of ozone through the 21st century. The participating CCMs are listed in Table 1 and are described in detail in the cited literature.

[7] The horizontal resolution varies from 10° × 22.5° (ULAQ) to 2° × 2.5° (AMTRAC and GEOSCCM), the location of the upper boundary from being centered at 10 hPa (E39C) to 10^{-6} hPa (WACCM), and the number of vertical levels ranges from 26 (ULAQ) to 71 (CMAM). The dynamics in all CCMs is determined by solving the "primitive" equations, except for ULAQ which is a quasi-geostrophic model. All CCMs consider gas-phase chemistry and heterogeneous chemistry on aerosols and on polar stratospheric clouds (PSCs), but different PSCs, dehydration, and denitrification schemes are used. All CCMs include feedbacks of the chemical tendencies of ozone and H_2O fields on radiation, and hence dynamics and transport of chemical species, but the coupling of other simulated GHGs with radiation varies among the models. The main features as well as the characteristics of the simulations of the past from the participating CCMs are summarized by *Eyring et al.* [2006].

[8] Each of the participating CCMs provided at least one long-term simulation where

1. The surface concentrations of the greenhouse gases carbon dioxide (CO_2), methane (CH_4), and nitrous oxide (N_2O) follow the Intergovernmental Panel on Climate Change (IPCC) Special Report on Emissions Scenarios (SRES) GHG scenario A1B (medium) [*IPCC*, 2000].

2. The surface halogens (chlorofluorocarbons (CFCs), hydrochlorofluorocarbons (HCFCs), and halons) are pre-

Table 1. A Summary of the Chemistry-Climate Models Used in This Study, Including the External Forcings and Representation of Quasibiennial Oscillation Used in the Model Simulations[a]

Model	Investigators	Domain/Resolution	Runs	SSTs	Solar Variability	QBO	Reference
AMTRAC	J. Austin, R.J. Wilson	2° × 2.5°, 8 L, 0.0017 hPa	3 × REF1[b], 1960–2004	J. Hurrell (personal communication, 2005)	*Lean* [2000]	NO	*Austin et al.* [2006]; *Austin and Wilson* [2006]
			3 × REF2[c], 1990–2099	Geophysical Fluid Dynamics Laboratory coupled atmosphere-ocean model	repeated 1950–2005 data	NO	
CCSRNIES	H. Akiyoshi, T. Nagashima, M. Yoshiki	T42, 34 L, 0.01 hPa	1 × REF1, 1980–2004	HadISST1 [*Rayner et al.*, 2003]	*Lean et al.* [1997]	forced	*Akiyoshi et al.* [2004]; *Kurokawa et al.* [2005]; *Shiogama et al.* [2005]
			1 × REF2, 1980–2050	CCSR/NIES/FRCGC coupled atmosphere-ocean model [*Shiogama et al.*, 2005]	NO	NO	
CMAM	D. Plummer, J. Scinocca, T. Shepherd	T32, 71L, 0.0006 hPa	1 × REF1, 1960–2004	HadISST1 [*Rayner et al.*, 2003]	NO	NO	*Beagley et al.* [1997]; *de Grandpré et al.* [2000]
			3 × REF2, 1960–2099	coupled version of the Canadian general circulation model (GCM); the three members all use a different realization of the SSTs from the coupled model	NO	NO	
E39C	M. Dameris, V. Eyring, V. Grewe, M. Ponater	T30, 39L, 10 hPa	3 × REF1, 1960–1999	HadISST1 [*Rayner et al.*, 2003]	*Lean et al.* [1997]	forced	*Dameris et al.* [2005, 2006]
			4 × SCN2, 2000–2019	HadGEM1 [*Johns et al.*, 2006]	solar cycles from the late 1950s to the 1970s	forced (1960s to 1970s)	
GEOSCCM	A. Douglass, P. Newman, S. Pawson, R. Stolarski	2° × 2.5°, 55 L, 0.01 hPa	1 × REF1[d], 1960–2003	HadISST1 [*Rayner et al.*, 2003]	NO	NO	*Stolarski et al.* [2006b]
			1 × REF2, 2000–2050	HadGEM1 [*Johns et al.*, 2006]	NO	NO	
MAECHAM4 CHEM	C. Brühl, M. Giorgetta, E. Manzini, B. Steil	T30, 39 L, 0.01 hPa	1 × REF1, 1980–1999	HadISST1 [*Rayner et al.*, 2003]	*Lean et al.* [1997]	forced	*Manzini et al.* [2003]; *Steil et al.* [2003]
			1 × REF2, 1 × SCN2, 2000–2019	HadCM3 [*Johns et al.*, 2006]	NO, solar cycles from the late 1950s to 1970s	NO, forced	
MRI	K. Shibata, M. Deushi	T42, 68 L, 0.01 hPa	1 × REF1, 1980–2004	HadISST1 [*Rayner et al.*, 2003]	*Lean et al.* [1997]	internally generated	*Shibata and Deushi* [2005]; *Shibata et al.* [2005]
			1 × REF2, 1980–2050	MRI-CGCM2.3 coupled atmosphere-ocean model [*Yukimoto et al.*, 2005]	NO	internally generated	
SOCOL	E. Rozanov, M. Schraner	T30, 39 L, 0.01 hPa	1 × REF1, 1980–2004	HadISST1 [*Rayner et al.*, 2003]	*Lean* [2000]	Forced	*Egorova et al.* [2005]; *Rozanov et al.* [2005]
			1 × REF2, 1980–2050	Atmospheric Model Intercomparison Projects (AMIP) II from 1980–2000 [*Taylor et al.*, 2000] and HadGEM1 from 2001–2050 [*Johns et al.*, 2006]	NO	NO	
ULAQ	E. Mancini, G. Pitari	10° × 22.5, 26 L, 0.04 hPa	1 × REF1[e], 1960–2004	HadISST1 [*Rayner et al.*, 2003]	NO	NO	*Pitari et al.* [2002]
			1 × REF2, 1980–2050	HadGEM1 [*Johns et al.*, 2006] up to 2019; repeated 2010–2019 cycle after 2019	NO	NO	

Table 1. (continued)

Model	Investigators	Domain/Resolution	Runs	SSTs	Solar Variability	QBO	Reference
UMSLIMCAT	M. Chipperfield, W. Tian	2.5° × 3.75°, 64 L, 0.01 hPa	1 × REF1, 1980–1999	AMIP II [*Gates et al.*, 1999]	NO	internally generated [*Tian et. al.*, 2006]	*Tian and Chipperfield* [2005]
			1 × REF2, 1980–2020	HadGEM1 [*Johns et al.*, 2006]	NO	internally generated	
WACCM (version 3)	R. Garcia, A. Gettelman, D. Kinnison, D. Marsh, F. Sassi	4° × 5°, 66 L, 4.5 × 10^{-6} hPa	3 × REF1[b] 1950–2003	J. Hurrell (personal communication, 2005)	www.sec.noaa.gov	NO	*Garcia et al.* [2007]
			3 × REF2, 1980–2050	CAM3 coupled atmosphere-ocean model	NO	NO	

[a]For grid point models the horizontal resolution is given in degrees latitude × longitude, and for spectral models as T30, T32, and T42 corresponding to the triangular truncation of the spectral domain with 30, 32, and 42 wave numbers, respectively. The number of vertical levels and the pressure level of the models' upper boundary is given in addition. The past simulations ("REF1") and the future simulation ("REF2" or "SCN2") are described by *Eyring et al.* [2005b]. All forcings can be downloaded from the Chemistry-Climate Model Validation activity (CCMVal) Web site at http://www.pa.op.dlr.de/CCMVal/. Changes in halogen concentrations in the "future" simulations are prescribed following the Ab scenario [*WMO/UNEP*, 2003; Table 4B-2] and greenhouse gases (GHGs) are based on the Intergovernmental Panel on Climate Change (IPCC) Special Report on Emissions Scenarios (SRES) scenario A1B (medium) [*IPCC*, 2000] in all simulations. Sulfate surface area densities beyond 1999 are fixed at 1999 conditions (volcanically clean conditions).
[b]REF1 but with sea surface temperatures (SSTs) from J. Hurrell (personal communication, 2005) and without Quasibiennial Oscillation (QBO).
[c]REF2 with solar cycle.
[d]REF1 without QBO, solar cycle, and volcanic eruptions.
[e]REF1 without QBO and solar cycle.

scribed according to the Ab scenario of *WMO/UNEP* [2003].

3. Sea surface temperatures (SSTs) and sea ice distributions are taken, if available, from IPCC AR4 simulations made with the coupled ocean-atmosphere models upon which the CCMs are based. Otherwise, SSTs and sea ice distributions are taken from a simulation with the UK Met Office Hadley Centre coupled ocean-atmosphere model HadGEM1 [*Johns et al.*, 2006]. For both options the data set is consistent with the IPCC SRES GHG scenario A1B (medium). The one notable exception is that in ULAQ a repeating 10-year cycle of SSTs from 2010 to 2019 was used for all subsequent decades after 2019. Note that none of the CCMs whose results are used in this paper was run with a coupled ocean or sea ice, since the inclusion of coupled chemistry already requires very large computational resources.

[9] These simulations generally follow the specifications of either the CCMVal reference simulation (REF2) or the CCMVal sensitivity simulation (SCN2) [*Eyring et al.*, 2005b]. In REF2 only anthropogenic forcings are considered and natural forcings such as solar variability are excluded. A quasibiennial oscillation (QBO) is only included in the model simulations that internally simulate the QBO. To assess the role of natural variability, the CCMVal sensitivity simulation, SCN2, includes a repeating solar cycle under volcanically clean aerosol conditions. All other forcings are as in REF2. The QBO in SCN2 is either internally forced or assimilated [*Giorgetta and Bengtsson*, 1999]. The model simulations and the forcings employed in each of the CCM simulations are summarized in Table 1.

[10] In this study the reference simulations of the past (REF1) are included only if they extend further back in time than the future simulations. The future simulation starts later than the REF1 simulation in AMTRAC (1990), in E39C, GEOSCCM, and MAECHAM4CHEM (2000), and in ULAQ and WACCM (1980), see Table 1. Some CCMs ran multiple future simulations with the same boundary conditions but slightly different initial conditions (AMTRAC, E39C, and WACCM). CMAM also provided multiple future simulations, but in contrast to all other CCMs, CMAM was forced with different realizations of the SSTs from a simulation with a coupled version of the Canadian general circulation model (GCM). In general, the variability between ensembles from a single model forced with the same SSTs is much smaller than the intermodel differences [see also *Austin and Wilson*, 2006; *Dameris et al.*, 2006]. The spread of the CMAM ensemble, forced by different SSTs (but from the same coupled GCM), is larger than the spread of the other model ensembles, but with the time filtering employed here it is still generally much smaller than the intermodel differences. Given the smaller spread among ensembles than among models, only one ensemble member from each CCM is used in the next sections, except for the analyses of total column ozone anomalies in section 4, which makes use of all simulations and all ensemble members.

3. Changes in Major Factors Affecting Stratospheric Ozone

[11] Before examining the projected ozone evolution from the CCMs we investigate the simulated changes in

quantities that influence ozone recovery. We focus here on changes in the simulated stratospheric halogens (section 3.1), temperature (section 3.2), and water vapor (section 3.3). Changes in other factors that could influence ozone in the future (e.g., stratospheric circulation, NO_y) are only briefly discussed in section 3.4.

3.1. Stratospheric Halogens

[12] From about 1980 to the mid 1990s observations showed a negative trend in globally averaged total ozone. It is generally accepted that an increase in stratospheric chlorine and bromine loading was the major cause of this trend [*WMO/UNEP*, 2007]. Therefore it is expected that future halogen loading will be a major factor determining the future evolution of ozone. The simulations used in this study follow a common scenario for surface halogen mixing ratios (see section 2). Nevertheless, there are differences in the simulated timing and magnitude of stratospheric inorganic chlorine (Cl_y) and bromine (Br_y) in the CCMs, which are discussed here.

[13] All models, except MRI (see discussion below), show Cl_y in the midlatitude lower stratosphere increasing rapidly during the 1980s and early 1990s, peaking in the late 1990s, and decreasing at a slower rate from the early 2000s onward, see Figure 1a. The time series in Figure 1, as well as all other time series shown in subsequent figures, are smoothed by applying a 1:2:1 filter iteratively 30 times (equivalent to a Gaussian filter with a 21 year 1/2 amplitude response). The line colors and styles in all figures are the same as those used in the CCM evaluation of *Eyring et al.* [2006], and are based on comparisons of stratospheric transport diagnostics, temperatures and Cl_y with observations. The CCMs shown with solid curves are those that are in general in good agreement with the observations considered by *Eyring et al.* [2006]. In polar regions (Figure 1c), the same time evolution is simulated, but compared to midlatitudes the peak occurs slightly later in most CCMs, consistent with around 1 year older age of air simulated in polar regions [see *Eyring et al.*, 2006, Figure 10]. While there is agreement among the majority of the CCMs concerning the shape of the Cl_y time evolution curve, there are large variations in the simulated peak Cl_y and the date when Cl_y returns to 1980 values. Peak Cl_y ranges from less than 1 ppb (E39C) to 3 ppb (AMTRAC) in midlatitudes and from 1 ppb (SOCOL) to over 3.5 ppb (AMTRAC) in polar regions (Cl_y at 80°N in March in the CCMs looks similar to the Cl_y at 80°S in October). Disregarding the results from MRI, the date Cl_y returns to 1980 values (Figures 1b and 1d) ranges from around 2035 (CMAM, SOCOL, and WACCM) to 2050 (AMTRAC and ULAQ) in midlatitudes and from before 2040 (SOCOL) to around 2060 (AMTRAC) in polar regions. In general, CCMs with lower peak Cl_y values predict Cl_y to decrease to pre-1980 values earlier than CCMs with higher peak values in the polar regions. This later return to 1980 for higher peak values is consistent with the theoretical calculations of equivalent effective stratospheric chlorine (EESC) by *Newman et al.* [2006], where the recovery date is later for larger peak values. Given the large range of simulated Cl_y, and expected close link between Cl_y and ozone, an important question is which Cl_y simulations are most realistic. The symbols in Figure 1a are from an analysis of spaceborne measurements of inorganic chlorine (D. Lary et al., Variations in stratospheric inorganic chlorine between 1991 and 2006, submitted to Geophysical Research Letters, 2007). The symbols in Figure 1c show estimates of Cl_y in the Antarctic lower stratosphere in spring from measurements from the Upper Atmospheric Research Satellite (UARS) satellite in 1992 and the Aura satellite in 2005, yielding values around 3 ppb [*Douglass et al.*, 1995; *Santee et al.*, 1996] and around 3.3 ppb [*WMO/UNEP*, 2007, Figures 4–8], respectively. As discussed by *Eyring et al.* [2006], the polar observations indicate that the majority of the models underestimate Southern Hemisphere polar Cl_y and that in several CCMs the peak Cl_y at 80°S is around or less than 2.5 ppb. This is most severe in E39C and SOCOL, which simulate springtime peak Cl_y of less than 1.5 ppb over Antarctica, which is clearly unrealistic. In midlatitudes, there is still a tendency for CCMs to underestimate Cl_y, although two CCMs (AMTRAC and MRI) overestimate Cl_y.

[14] The differences in simulated Cl_y, which are largest in the polar lower stratosphere, were shown by *Eyring et al.* [2006] to be primarily related to transport differences. However, transport differences do not explain all of the differences in Cl_y. The UMSLIMCAT run, which shows a slightly different time evolution of Cl_y than most CCMs, had not fully spun up by 1980 and did not capture the correct stratospheric lag compared to the troposphere until around 1985. In AMTRAC, the Cl_y production rates are parameterized according to the age of air and the tropospheric source molecules as a function of time. The parameterization was designed to simulate correct values of Cl_y in the upper stratosphere, but has in practice led to far too much Cl_y in the lower and middle stratosphere away from the polar regions, see for example Figures 1a and 1c.

[15] As mentioned above, the evolution of Cl_y in the 21st century in MRI is very different from that of the other models, and the peak Cl_y does not occur until after 2015. The total chlorine Cl_{tot} (sum of inorganic and organic) in this model also does not peak until around 2015, and the time lag from the tropospheric total chlorine is around 15 years (not shown). The very slow Cl_y increase in MRI comes from the combined effect of the diffusive nature of the transport scheme and a weak Brewer-Dobson circulation. The continued increase of Cl_y and Cl_{tot} is unrealistic, as observations show upper stratospheric Cl_{tot} has peaked and is currently decreasing [*Anderson et al.*, 2000; *Waugh et al.*, 2001; *Froidevaux et al.*, 2006]. This causes us to place low confidence in the long-term ozone projections given by the MRI simulation.

[16] The above discussion has focused on the simulated Cl_y, but it is also important to consider Br_y. Although the concentration of Br_y is much less than Cl_y, the bromine catalytic cycles involved in ozone loss are more efficient than those of chlorine. To account for this, the Br_y contribution is usually scaled by a factor α (which is between 50 and 70, *WMO/UNEP* [2007]), and the combined impact of chlorine and bromine is represented by $Cl_y + \alpha Br_y$, which we refer to as "equivalent stratospheric chlorine" or "ESC". ESC differs from EESC as it is calculated from stratospheric concentrations of Cl_y and Br_y, whereas EESC is based on tropospheric concentrations of source gases and age of air considerations. The simulated variation of ESC, calculated with $\alpha = 60$, relative to its 1980 value in the Antarctic lower stratosphere is shown in Figure 1e. The

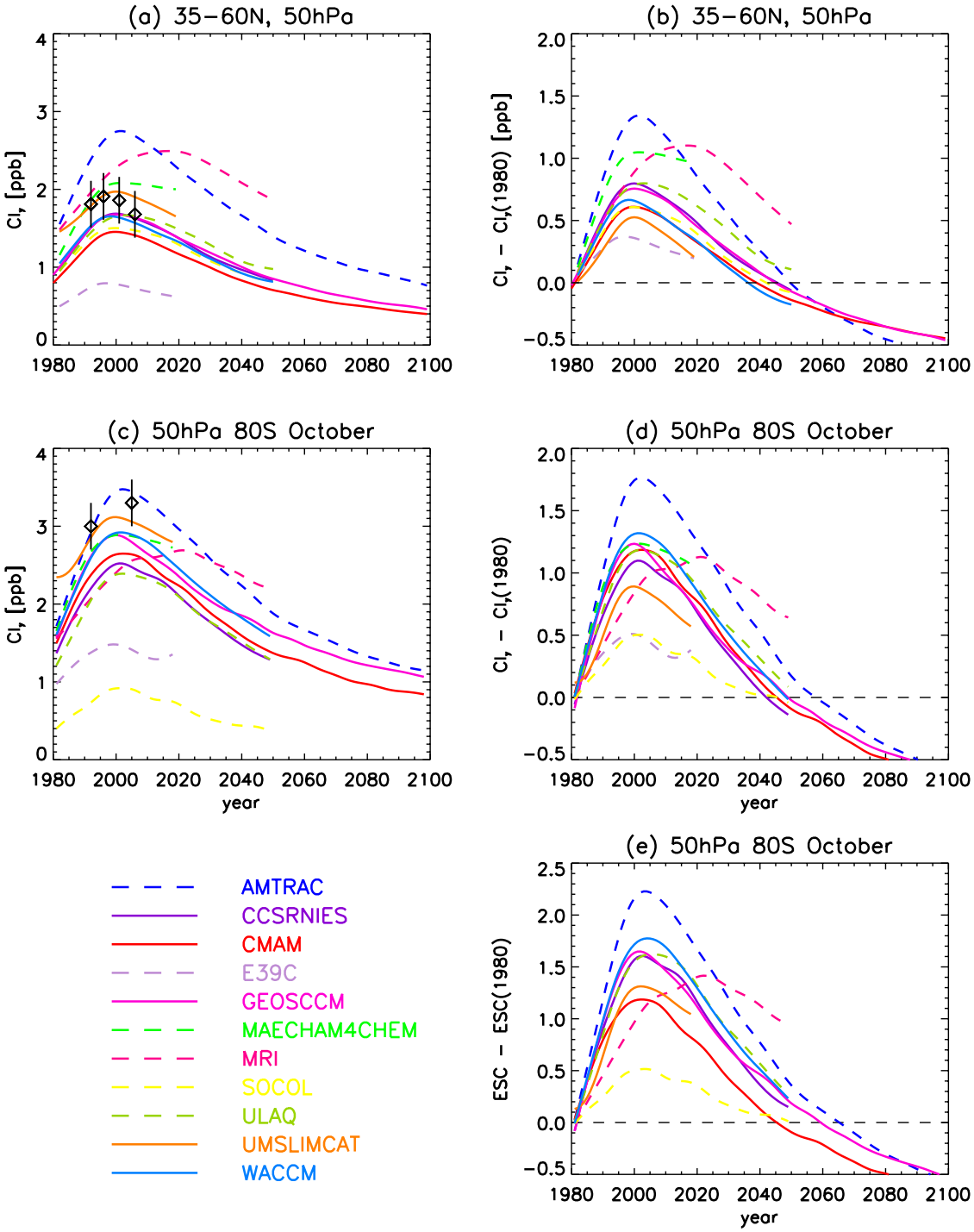

Figure 1. Zonal mean values of total inorganic chlorine (Cl_y in ppb) at 50 hPa for (a) annual mean 35–60°N and (c) October at 80°S. (b and d) Difference in Cl_y from that in 1980. (e) Difference in equivalent stratospheric chlorine (ESC) (Cl_y + 60Br_y) from that in 1980. Solid and dashed curves show smoothed data derived by applying a 1:2:1 filter iteratively 30 times. Symbols in Figures 1a and 1c show observational estimates of Cl_y; see text for details.

number of models shown in Figure 1e is less than in Figures 1a–1d as Br_y was not included in E39C and MAECHAM4CHEM and was not archived in others. In CMAM the abundance of tropospheric halons is fixed with time, and Br_y used in the ESC calculation is a decadal mean (2009–2019) to account for interannual variability in the transport into the polar lower stratosphere. In SOCOL Br has not been archived and was not included in the calculation of Br_y. The evolution of ESC closely resembles the variation of Cl_y although the date that ESC returns to its

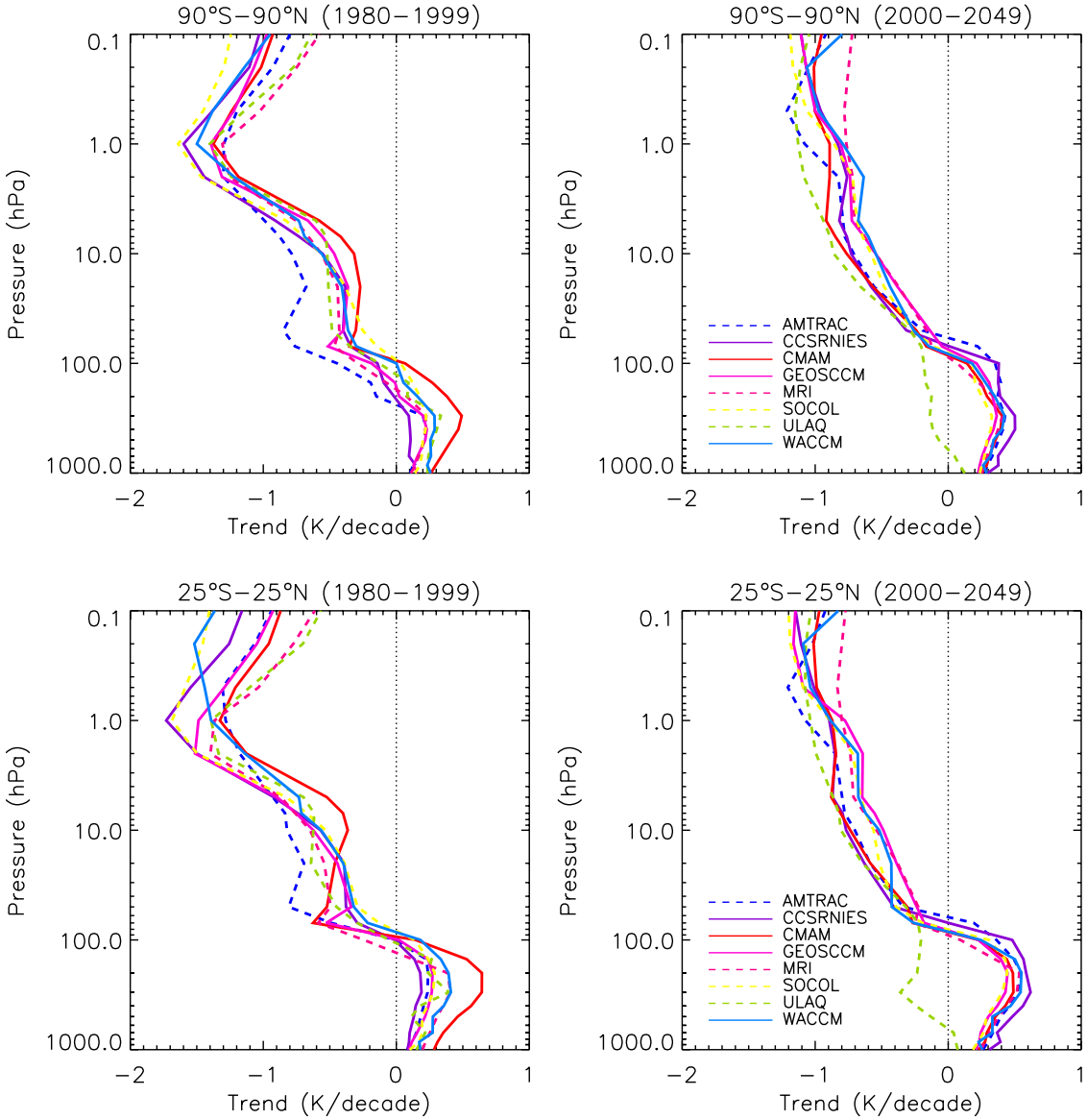

Figure 2. Vertical distribution of annual mean global (90°S to 90°N, top row) and tropical (25°S to 25°N, bottom row) temperature trends from 1980 to 1999 (left) and 2000 to 2049 (right) from the eight chemistry-climate models (CCMs) that were run at least through 2050.

1980 value is later than that for Cl_y by 5–10 years, because of the slow decay of source halons. However, conclusions regarding intermodel variations in Cl_y also apply for ESC.

[17] The differences in the simulated timing and peak of Cl_y or ESC in the CCM simulations discussed above are expected to cause differences in the ozone projections. This is further discussed in section 4.

3.2. Temperatures

[18] In addition to stratospheric halogen concentrations, changes in stratospheric temperatures are expected to have a large impact on the future evolution and recovery of stratospheric ozone. Ozone loss depends on the rate of chemical reactions and the formation of PSCs, both of which depend on temperature. The CCMs examined here are able to reproduce the observed long-term global mean lower-stratospheric temperature trend resulting from GHG increases and stratospheric ozone depletion over the last 2 decades [*Eyring et al.*, 2006]. All CCMs, except MRI, reproduce the stronger cooling trend in the Southern Hemisphere high latitudes compared to the north, which is expected because of the larger Southern Hemisphere polar ozone loss in spring. This gives us some confidence that the temperature feedback from changes in GHGs, and the ozone radiative dynamical feedback, are well captured in the CCMs and suggests that CCMs are suitable tools for projecting stratospheric temperatures under a given GHG and halogen emission scenario, which is a prerequisite for predicting ozone.

[19] All of the eight CCMs that ran at least through 2050 show stratospheric global cooling in the periods 1980 to 2000 and 2000 to 2049 (Figure 2). For each CCM, the annual average temperature is averaged over the particular region and a linear trend in K/decade is computed at each

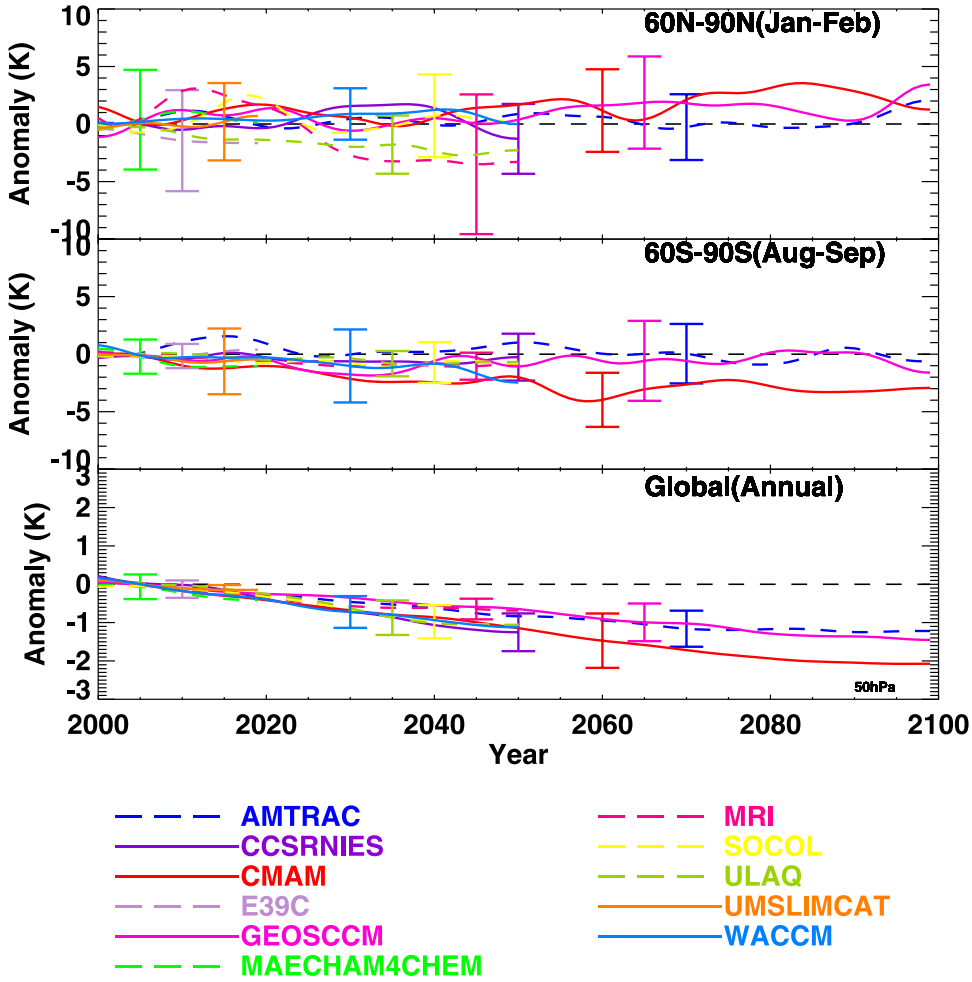

Figure 3. Modeled time series of monthly mean temperature anomalies at 50 hPa from the CCMs. Temperature anomalies are calculated with respect to a mean reference period between 2000 and 2010 using 2-month averages for January to February in the polar Northern Hemisphere (60°–90°N, top), August to September in the polar Southern Hemisphere (60°–90°S, middle), and annual averages for the global anomalies (bottom). Time series have been smoothed as in Figure 1. Error bars denote plus or minus 2 standard deviations of the individual years from the smoothed curve.

pressure level from the unsmoothed model data. An increase in the concentrations of GHGs, in particular CO_2, as assumed in the simulations presented here, is expected to cool the middle atmosphere, with a maximum cooling around the stratopause [*Jonsson et al.*, 2004; *Sigmond et al.*, 2004; *Schmidt et al.*, 2006; *Fomichev et al.*, 2007]. Consistently, in the stratosphere all CCMs show a cooling trend between 2000 and 2049, which increases with altitude up to 1 K/decade above 1 hPa. A comparison of the past (1980–1999; Figure 2, left) and future (2000–2049; Figure 2, right) temperature trends shows similar results at around 20 hPa. However, both in the upper and lower stratosphere the cooling is significantly larger between 1980 and 1999 compared to the period between 2000 and 2049.

[20] Between 2000 and 2049, all CCMs show a warming in the troposphere due to GHG increases, with the exception of the ULAQ model. The cooling in the ULAQ model in the troposphere may be due to at least two factors: (1) After 2019 a repeating 10 year cycle that uses the values from 2010 to 2019 for all subsequent decades has been used for SSTs, which underestimates the surface warming in the ULAQ simulation between 2020 and 2050, and (2) the convective heating in ULAQ may be insufficient to link the surface warming to the free troposphere. In all other CCMs the largest warming is found in the middle to upper troposphere, in general agreement with coupled atmospheric-ocean climate models [*Cordero and de Forster*, 2006].

[21] Global temperatures at 50 hPa decrease further until 2100 because of continuous GHG increases in the simulations (Figure 3). The temperature anomalies are calculated by subtracting a 2000–2010 annual cycle average. Linear temperature trends in K/decade are calculated for each model using data between 2000 and the end of the particular model simulation (Table 2). In addition, Table 3 shows temperature trends for two different periods (2000–2049 and 2050–2099) for three different latitude bands (60°N–90°N; 60°S–90°S; 90°N–90°S). The statistical significance of the trend being nonzero is evaluated at the 95% confidence level, where a lag-1 autocorrelation is used to account for the nonindependence of the residual values about the

Table 2. Decadal Linear Temperature and Water Vapor Trends at 50 hPa in Different Regions for Each CCM Using Data Between 2000 and the End of the Particular Model Simulation[a]

Model	Trend Period	Polar NH (60°–90°N)		Polar SH (60°–90°S)		Global (90°S–90°N)	
		Temperature, K/decade	H_2O, ppmv/decade	Temperature, K/decade	H_2O, ppmv/decade	Temperature, K/decade	H_2O, ppmv/decade
AMTRAC	2000–2099	0.035	0.11*	−0.08	0.074*	−0.15*	0.090*
CCSRNIES	2000–2049	0.15	0.08*	−0.18	0.057*	−0.31*	0.063*
CMAM	2000–2099	0.23	0.054*	−0.30*	0.059*	−0.24*	0.055*
E39C	2000–2019	−2.2	0.11	0.20	−0.036	−0.25*	0.14
GEOSCCM	2000–2099	0.21	0.072*	0.043	0.041*	−0.16*	0.057*
MAECHAM4CHEM	2000–2019	−0.37	0.051	−1.1	−0.034	−0.29*	0.058
MRI	2000–2049	−1.3	0.043*	−0.24	0.028*	−0.17*	0.036*
SOCOL	2000–2049	0.015	0.29*	−0.21	0.16*	−0.27*	0.22*
ULAQ	2000–2049	−0.52*	−0.14*	−0.18	−0.076*	−0.29*	−0.14*
UMSLIMCAT	2000–2019	0.93	−0.004	0.67	0.045	−0.15*	−0.025
WACCM	2000–2049	0.18	0.11*	−0.51	0.052*	−0.26*	0.061*

[a]In the polar regions the temperature trends are calculated using 2 month averages between January and February in the Northern Hemisphere (NH) (60°–90°N), and August to September in the Southern Hemisphere (SH) (60°–90°S). Polar water vapor trends are calculated using 2 month averages between November and December in the Northern Hemisphere, and May to June in the Southern Hemisphere. Annual averages are used for the global trends. Trend values are labeled with an asterisk if they are statistically significant at the 95% confidence level.

trend line. The simulated global temperature trends are all statistically significant over the first and second half of the 21st century. The eight CCMs that ran at least through 2050 show an average global cooling trend of 0.24 K/decade during the period 2000–2049, and the three CCMs that ran through 2100 show an average global cooling trend of 0.15 K/decade during the period 2050–2099. However, this should not be interpreted as a slow down of the cooling trend in the second half of the century, because only two out of the three CCMs that ran through 2100 simulate a smaller cooling trend in the second half of the century than in the first, but one CCM simulates a larger cooling trend (see Table 3).

[22] In the polar regions, 2-month averages for January to February in the Northern Hemisphere and for August to September in the Southern Hemisphere are examined to look at temperature changes due to GHG increases before the ozone depletion season. In the Northern Hemisphere polar region (60°N–90°N) at 50 hPa, the model temperature anomalies generally range between ±4 K and are dominated by interannual variability. There are no consistent temperature trends at 50 hPa among the CCMs, with some of the trends being positive and others negative (see also Tables 2 and 3). During 2000–2049 only one out of the eight model simulations (ULAQ) and during the period 2050–2099 none of the three simulations shows a statistically significant trend. In the Southern Hemisphere polar region (60°S–90°S), the interannual variability of ±3 K is smaller than in the Northern Hemisphere. During the first part of the century, all CCMs simulate a cooling (on average 0.27 K/decade), but in only one out of the eight model simulations (CMAM) is this cooling trend statistically significant. The three CCMs that ran through 2100 show an average cooling trend of 0.05 K/decade in the period 2050–2100, but none of these trends are statistically significant.

[23] Global annual mean cooling trends of around 1 K/decade over the period 2000 to 2050 in the upper stratosphere and of around 0.25 K/decade in the lower extra-polar stratosphere (Figure 2) due to increasing GHGs are expected to slow down gas-phase ozone loss cycles and increase ozone in these regions [e.g., *Haigh and Pyle*, 1982; *Rosenfield et al.*, 2002; *Jonsson et al.*, 2004]. In contrast, a decrease in temperature in the polar lower stratosphere increases the likelihood of the formation of PSCs and, given

Table 3. Model-Calculated Linear Temperature Trends at 50 hPa From 2000 to 2049 and 2050 to 2099 in K/decade for the CCMs That at Least Ran Through 2050 and a Multimodel Average in Different Regions[a]

Model	Polar NH (60°–90°N) January and February		Polar SH (60°–90°S) August to September		Global (90°S–90°N) Annual Mean	
	2000–2049	2050–2099	2000–2049	2050–2099	2000–2049	2050–2099
AMTRAC	−0.055	0.13	−0.06	−0.150	−0.20 *	−0.10*
CCSRNIES	0.15	—	−0.18	—	−0.31*	—
CMAM	0.13	0.17	−0.62*	−0.063	−0.24*	−0.19*
GEOSCCM	0.02	0.17	−0.19	0.049	−0.14*	−0.17*
MRI	−1.3	—	−0.24	—	−0.17*	—
SOCOL	0.015	—	−0.19	—	−0.27*	—
ULAQ	−0.52*	—	−0.18	—	−0.29*	—
WACCM	0.18	—	−0.51	—	−0.26*	—
Model Average	−0.12	0.16	−0.27	−0.05	−0.24*	−0.15*

[a]In the polar regions the temperature trends are calculated using 2 month averages between January and February in the Northern Hemisphere (60°–90°N), and August to September in the Southern Hemisphere (60°–90°S). Annual averages are used for the global trends. Trend values are labeled with an asterisk if they are statistically significant at the 95% level.

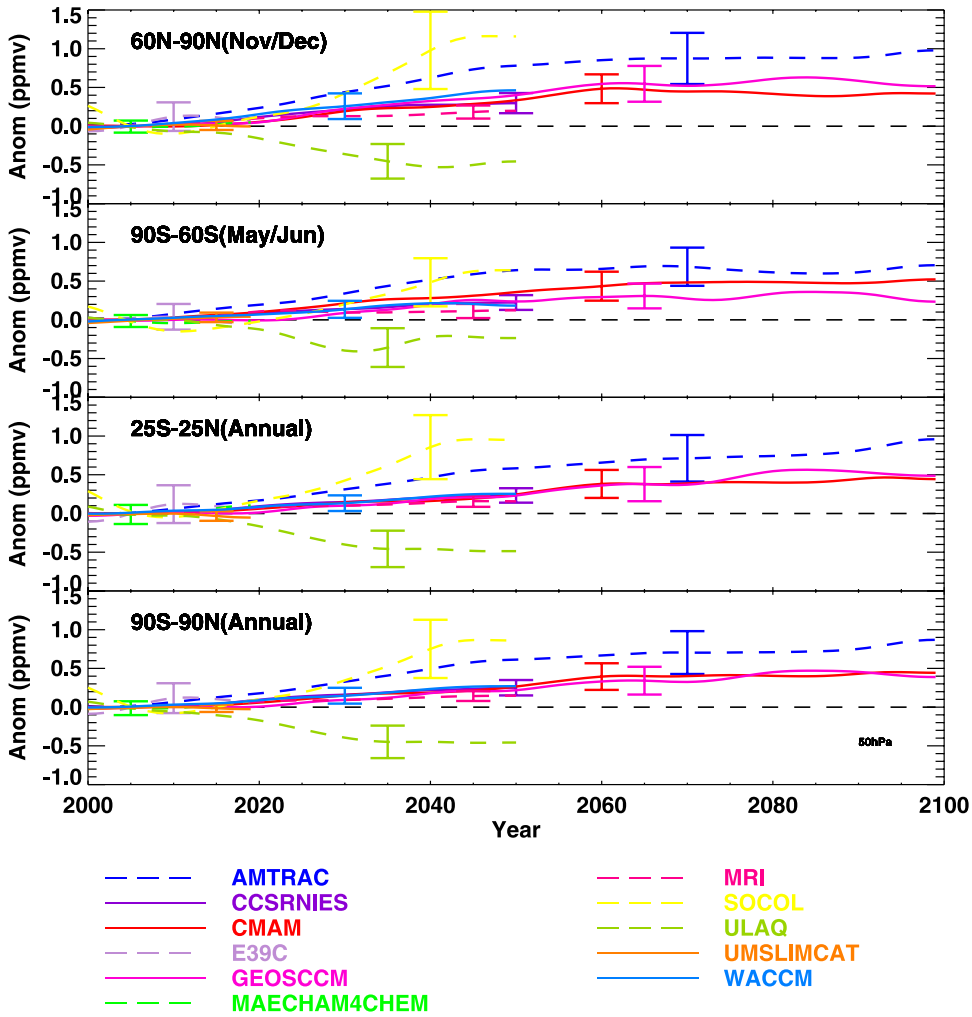

Figure 4. Modeled time series of monthly mean water vapor anomalies at 50 hPa from the CCMs. Water vapor anomalies are calculated with respect to a mean reference period between 2000 and 2010 using 2-month averages for November to December in the polar Northern Hemisphere (60°–90°N), May to June in the polar Southern Hemisphere (60°–90°S), and annual averages for the tropical and global anomalies. Time series have been smoothed as in Figure 1. Error bars denote plus or minus 2 standard deviations of the individual years from the smoothed curve.

sufficient halogen loading, increases chemical ozone loss in the Arctic [*Rex et al.*, 2004; *Tilmes et al.*, 2004]. In the Antarctic stratosphere, observations show that lower than average temperatures increase the severity of the ozone hole [*Newman et al.*, 2004; *Huck et al.*, 2005]. However, the CCMs simulate very small temperature trends in the first and second half of the 21st century in the polar regions in midwinter (Table 3), so more severe ozone losses due to further cooling of the polar lower stratosphere under the given greenhouse gas scenario are not expected.

3.3. Water Vapor

[24] The recovery of ozone could also be affected by changes in stratospheric water vapor [*Kirk-Davidoff et al.*, 1999; *Dvortsov and Solomon*, 2001; *WMO/UNEP*, 2007, chapter 5]. An increase in water vapor would increase hydrogen oxide (HO_X), and lead to increased ozone loss in the extrapolar lower and upper stratosphere, where HO_X dominates ozone loss [see *IPCC/TEAP*, 2005, Figure 1.11]. In addition to changing HO_X, an increase in water vapor would affect PSC formation and heterogeneous reactions in the CCMs, which could lead to increased springtime polar ozone loss [*Tabazadeh et al.*, 2000; *Stenke and Grewe*, 2005; *WMO/UNEP*, 2007]. It is therefore important to quantify the predicted change in water vapor from the CCMs.

[25] All CCMs (with the exception of ULAQ) show an increase in global and tropical annual mean lower-stratospheric water vapor, see Figure 4. A possible reason for a water vapor increase is a warming of the tropical tropopause in the models. Tropical tropopause temperatures from the models are not available for this study, but analysis of tropical temperatures at 100 hPa shows a positive trend in all CCMs except ULAQ (see Figure 2). In the ULAQ simulation the future tropical temperature trend at 100 hPa is negative rather than positive as in all other CCMs, and consistent with this, ULAQ shows negative trends in water vapor. Another contributor to the increase in stratospheric

water vapor is the prescribed increase of tropospheric methane concentrations (tropospheric CH_4 increases from 1761 ppbv in 2000 to 2399 ppbv in 2050 in the simulations) which results in an increase in water vapor produced by oxidation of methane. Overall, the stratospheric global mean water vapor trends through 2049 (less than 0.063 ppmv/decade or ~2%/decade in most CCMs) and through 2099 (0.09 ppmv/decade in AMTRAC; ~0.056 ppmv in CMAM and GEOSCCM) that are simulated by the CCMs are small (Table 2). These small trends are not expected to cause a significant delay of the recovery of the ozone layer [*Dvortsov and Solomon*, 2001; *Shindell*, 2001] or contribute to changes in total ozone amounts [*Stenke and Grewe*, 2005]. For example, *Dvortsov and Solomon* [2001] and *Shindell* [2001] estimated that a 10% per decade increase of stratospheric water vapor would delay the recovery of the ozone layer by about 10 to 15 years, so the ~2% per decade simulated in the current CCMs is expected to delay recovery by only around 2–3 years.

[26] Over the polar regions changes in water vapor are also not expected to have a large impact on ozone. Figures 4a and 4b show the changes in polar water vapor at the start of the winter season before dehydration occurs in the CCMs (November to December mean in the Northern Hemisphere and May to June mean in the Southern Hemisphere). Over the Arctic two out of the eight CCMs that ran through 2049 show an increase of 0.9 ppmv (AMTRAC) and 1.45 ppmv (SOCOL) by 2049, which could lead to an enhancement of PSCs and thus greater ozone loss than in the absence of the water vapor changes [*Tabazadeh et al.*, 2000]. However, *Stenke and Grewe* [2005] showed that a 1 ppmv water vapor perturbation results in only a small percentage change in zonally averaged total column ozone in Arctic spring. The increase in the other simulations by 2050 is smaller than 0.55 ppmv. Over Antarctica water vapor trends are smaller than over the Arctic and are therefore also not expected to have a large impact on ozone changes (Table 2). In addition, in the models where the present-day high-stratospheric halogen concentrations exceed those necessary to cause total loss in the Antarctic, a change in the chlorine activation through a change in heterogeneous effects has very limited impact on the simulated chemical ozone loss.

3.4. Other Factors

[27] Factors other than changes in halogens, temperatures, and water vapor could potentially change the evolution of ozone in the 21st century. Previous studies have highlighted the potential for changes in the stratospheric circulation [*Butchart and Scaife*, 2001] and N_2O [*Randeniya et al.*, 2002] to impact ozone recovery. We briefly discuss below the changes in these factors in CCM simulations examined here, but leave a detailed examination of these and other changes for future studies.

[28] Changes in the stratospheric circulation have the potential to change the evolution of ozone in the 21st century. A robust result of previous modeling studies is that an increase in GHGs leads to an increased stratospheric circulation and to increased tropical vertical velocities (upwelling) [*Butchart and Scaife*, 2001; *Butchart et al.*, 2006]. The increase in tropical upwelling leads to reduced transport timescales and a decrease in the mean age of air [*Austin and Li*, 2006; *Garcia et al.*, 2007]. Several of the CCMs examined here included an age of air tracer (AMTRAC, CMAM, GEOSCCM, MRI, ULAQ, and WACCM). In all except MRI the mean age of air decreases through the 21st century, with a decrease in mean age of air in the tropical middle stratosphere of around 0.25 years between 2000 and 2050. This implies that in these models there is an increase in the tropical upward mass flux from the troposphere. As pointed out by *Butchart and Scaife* [2001], an increase in this upward mass flux could accelerate the removal of chlorofluorocarbons (CFCs) and the reduction of stratospheric Cl_y, which would speed up ozone recovery. However, this effect is not represented in simulations which impose the tropospheric halogen concentrations. In contrast, in the tropical lower stratosphere the increase in tropical upwelling could decrease ozone in this altitude range (see further discussion in section 4.1). A strengthening of the Brewer-Dobson circulation might also increase polar downwelling, which would counteract the GHG-induced cooling of the polar stratosphere [*Manzini et al.*, 2003]. Through the above and other mechanisms, the increased circulation in the CCMs is likely to impact on ozone recovery. However, the quantitative impact of the increased tropical upwelling on ozone is still an open question that needs to be addressed in future studies.

[29] Increases in N_2O could impact the recovery of ozone by increasing the level of NO_x in the stratosphere [*Randeniya et al.*, 2002]. In the CCM simulations the surface concentration of N_2O, which follows IPCC SRES GHG scenario A1B, increases by around 16% between 1980 and 2050. Over the same period the stratospheric NO_y in the CCMs generally increases by around 10% or less (not shown). The smaller increase in NO_y than in N_2O is due to temperature decreases in the upper stratosphere [*Rosenfield and Douglass*, 1998]. This increase is expected to lead to a decrease in ozone in the middle stratosphere due to increased destruction by NO_x. However, the percentage decrease in ozone is expected to be much smaller than the percentage NO_y increase. For example, the 2D model calculations of *Randeniya et al.* [2002] and *Chipperfield and Feng* [2003] indicate that the maximum decrease in midlatitude ozone due to future increases in NO_y occurs around 30 km, and that a 10% increase in NO_y results in only around a 2–3% decrease in ozone at this altitude. Thus the increase in NO_y in the CCMs is not likely to be a major factor in the long-term evolution of ozone.

4. Projections of the Behavior of Ozone

[30] The projected ozone evolution is now examined for the beginning of the 21st century, the middle of the century and the end of the century. The ozone projections are assessed in terms of area-weighted monthly total column ozone anomalies over different latitude zones, as well as decadal changes in vertical ozone profiles between the 2040s and the 1980s.

4.1. Global and Midlatitude Ozone

[31] In the extrapolar regions the CCMs all show ozone losses in response to increasing ODSs in the annual means of monthly total column ozone anomalies in the last 2 decades of the 20th century, see Figure 5. The anomalies are calculated with respect to a 1980–1989 "detrended

mean annual cycle" by using a regression model applied to simulations over this period (for details see *Eyring et al.* [2006]). As with the previous time series plots (Figures 1, 3, and 4), these anomaly fields have been smoothed by applying a 1:2:1 filter iteratively 30 times, and some features near the ends of the curves are artifacts of this smoothing. There are some notable deviations from observations [see also *Eyring et al.*, 2006]; e.g., before 1980 three CCMs simulate stronger than observed total ozone anomalies (AMTRAC, GEOSCCM, and ULAQ) and between 1980 and 2004 two CCMs overestimate ozone trends (AMTRAC and MRI) in all extrapolar regions, whereas most models underestimate observed ozone trends in the midlatitudes, in particular in the Northern Hemisphere. In the tropics, nearly all CCMs show higher than observed ozone trends. The variability in the CCMs, which is partly removed by the smoothing of the time series in Figure 5, arises from internal dynamics and variations in prescribed

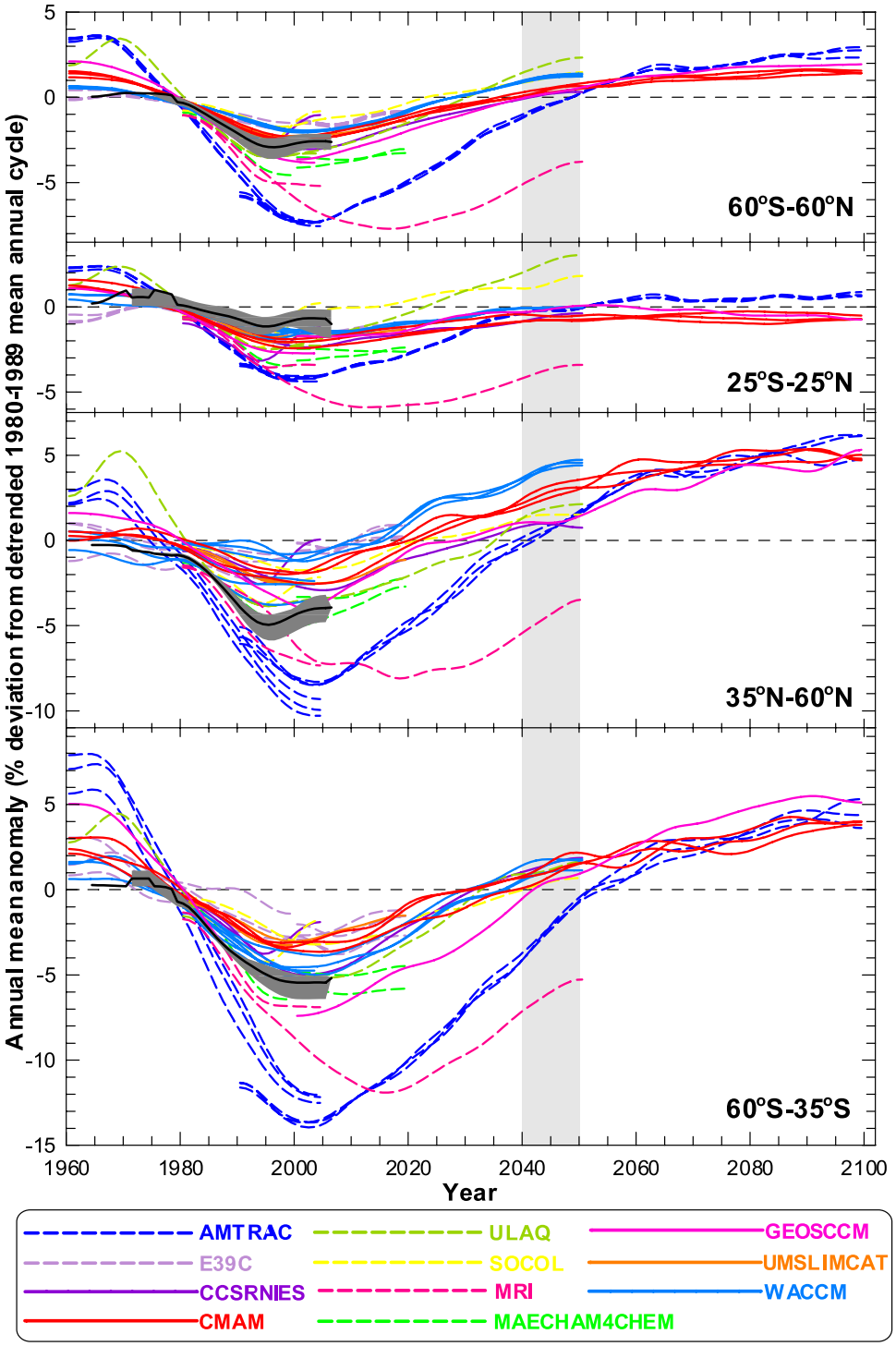

Figure 5

SSTs with time. Variability associated with the QBO and 11-year solar cycle is also included in some CCM simulations (see Table 1) and contributes to the interannual and longer time variations.

[32] The shape of the column ozone time evolution curve in the extrapolar regions is qualitatively similar in almost all CCMs. The lowest smoothed ozone occurs around 2000 with a broad minimum after which ozone slowly increases (Figure 5). Averaged between 60°N and 60°S, total column ozone is projected to increase in all CCMs between 2000 and 2020, with most of the increase of 1% to 2.5% occurring after 2010. Over midlatitudes, the majority of the models predict an increase of 1.5% to 3.5%, while over the tropics smaller ozone increases of less than 2% are projected by most models. The evaluation of the timing of ozone minima is obscured by the interannual variability. If smoothed CCM anomalies are used and, to avoid local ozone minima caused by Pinatubo, only minima after 1996 are considered, the CCMs predict that the minimum in 60°S and 60°N column ozone has already occurred (Figure 5).

[33] Although the general evolution of ozone is similar for all the models, there is a large spread in the magnitude of the predicted ozone anomalies. Much of this spread is due to two CCMs (AMTRAC and MRI), which show larger than observed ozone anomalies in the recent past and much larger ozone anomalies until 2050 than simulated by all other CCMs. The larger ozone anomalies in AMTRAC and MRI are consistent with larger than observed Cl_y in midlatitudes in AMTRAC and different time evolution of Cl_y in MRI (see Figure 1a and discussion in section 3.1). Differences in simulated Cl_y also explain some of the differences in ozone anomalies among the remaining CCMs. For example, E39C simulates only small trends in midlatitude Cl_y in the past and over the next 2 decades (Figures 1a and 1b) and also small ozone changes, whereas MAECHAM4-CHEM simulates a larger trend during the 1980s and 1990s in Cl_y and ozone than most CCMs, which better resembles observations (Figure 5).

[34] The simulated Cl_y in midlatitudes in most models decreases to its 1980 value between 2035 and 2050 (Figure 1b). This is consistent with projections of EESC [*WMO/UNEP*, 2003]. If no other factors played a role, it would be expected that ozone would increase to its 1980 values at the same time. However, if there are changes in temperature, transport or the abundance of other gases, ozone may return to 1980 values earlier or later than ODSs. All CCMs, except AMTRAC and MRI, predict midlatitude ozone to be on average higher than 1980 values between 2040 and 2050, with increases to 1980 values generally occurring between 2005 and 2035 over northern midlatitudes, and somewhat later over southern midlatitudes, between 2025 and 2040. The earlier return of northern midlatitude ozone to pre-1980 values is echoed in the hemispheric differences in ozone anomalies between 2040 and 2050 (0.5 to 5% in the Northern Hemisphere and −0.5 to 3% in the Southern Hemisphere). The two exceptions to the foregoing statements are AMTRAC and MRI which show a slower return of ozone to 1980 values such that ozone remains below 1980 values in 2040. The slower return of ozone to pre-1980 values in AMTRAC and MRI is consistent with the slower decrease of Cl_y to 1980 values (Figure 1b) in these models.

[35] The recovery of total column ozone to levels higher than would be expected from ODS concentrations alone (i.e., "super recovery" of ozone to levels higher than in 1980) is a result of increases in middle and upper stratospheric ozone. Figure 6 shows the change in decadal average stratospheric ozone from the 1980s to the 2040s, and all models (except MRI) show increases in ozone in the middle and upper stratosphere, with peak increases around 0.6–0.7 ppmv around 3–5 hPa. The increases in the middle and upper stratosphere are primarily due to strong cooling of the middle and upper stratosphere by increasing GHGs (see Figure 2 and section 3.2) [e.g., *Rosenfield et al.*, 2002; *Chipperfield and Feng*, 2003; *Fomichev et al.*, 2007].

[36] Changes in tropical total ozone differ from midlatitudes, and the majority of the CCMs predict total column ozone about the same or even somewhat less than 1980 values in 2040–2050 (Figure 5). In the vertical ozone changes this is reflected by a small decrease in tropical lower-stratospheric ozone from the 1980s to the 2040s in all CCMs (except in ULAQ where there is an increase in the lower stratosphere and a decrease between 15–30 hPa), which is not present in the midlatitudes (Figure 6). The decrease in lower-stratospheric ozone in the future is likely related to future increases in tropical upwelling (see section 3.4). A future increase in upwelling in the tropics would bring ozone poor air from the troposphere into the tropical lower stratosphere, thus decreasing ozone in this altitude region. At the same time increases in ozone in the upper stratosphere (due to cooling and slower ozone gas phase destruction reactions) might reduce the penetration of UV to the lower stratosphere reducing ozone production there (a reverse of the "self-healing" effect) [e.g., *Rosenfield et al.*, 2002; *Rosenfield*

Figure 5. Annual mean zonal mean total column ozone anomalies from CCMs (colored lines) and from four observational data sets (thick black line and gray shaded area show the mean and range of observed anomalies). Four observational data sets are taken from ground-based measurements (updated from *Fioletov et al.* [2002]), merged satellite data [*Stolarski and Frith*, 2006], the National Institute of Water and Atmospheric Research (NIWA) assimilated database [*Bodeker et al.*, 2005], and from Solar Backscatter Ultraviolet (SBUV, SBUV/2) retrievals (updated from *Miller et al.* [2002]). Area-weighted zonal mean time series are shown for the extrapolar region (60°S to 60°N), the equatorial region (25°S to 25°N), the northern midlatitude region (35°N to 60°N), and the southern midlatitude region (60°S to 35°S). Observational time series have been smoothed as in Figure 1. Light gray shading between 2040 and 2050 shows the period when stratospheric concentrations of halogens are expected to return to their 1980 values. Monthly anomalies were calculated by subtracting a detrended mean annual cycle, calculated over the period 1980–1989, from each time series. Annual cycle was detrended by fitting a regression model with seasonally dependent trends to the data and reconstructing the "1980" mean annual cycle using the stationary components of the regression model. For further details on the method for calculating the anomalies see *Eyring et al.* [2006].

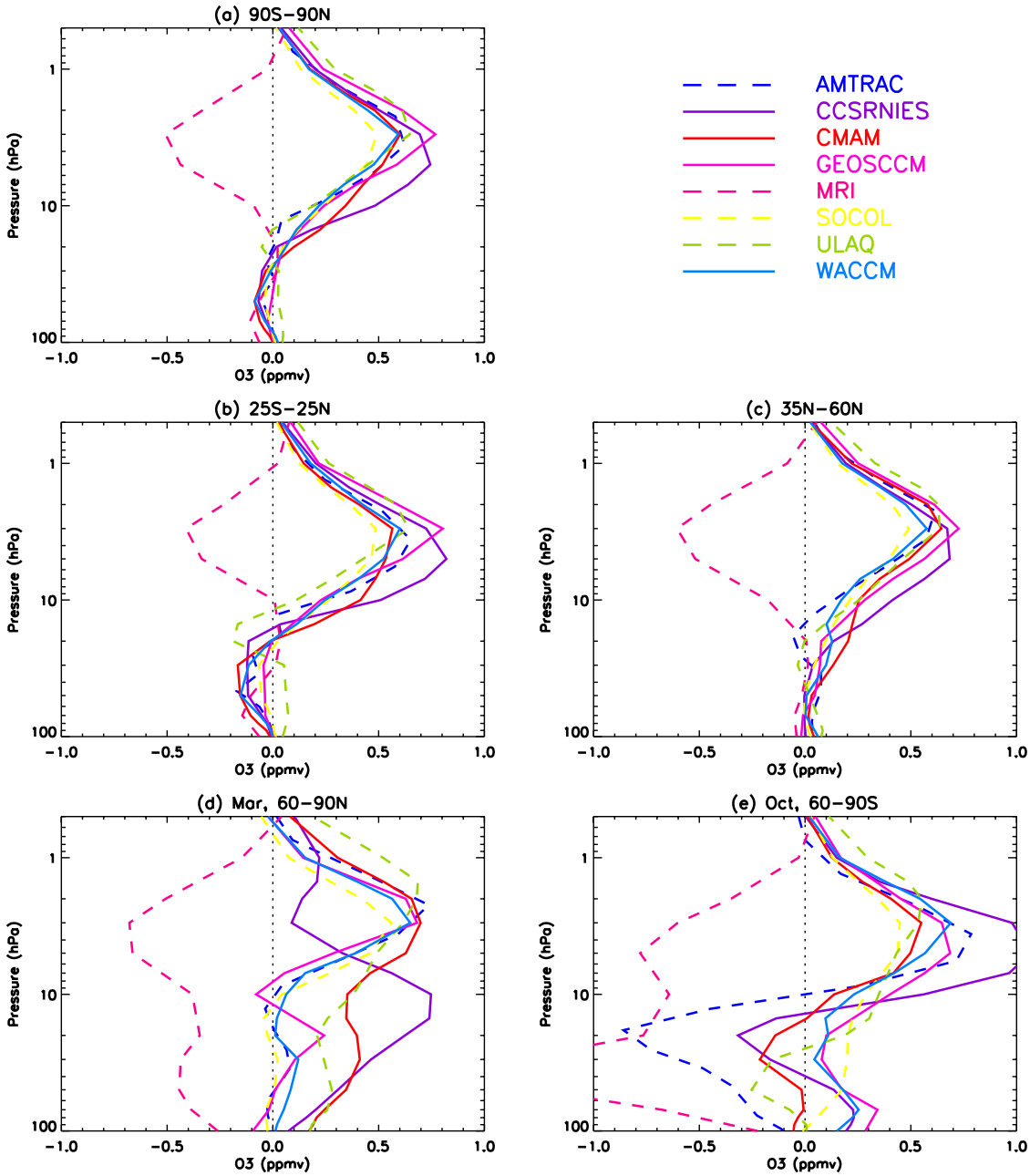

Figure 6. Decadal differences in ozone profiles between the 2040s (2040–2049) and the 1980s (1980–1989) for (a) global annual mean, (b) annual mean in the tropics, (c) annual mean in the midlatitude Northern Hemisphere, (d) March mean in the polar Northern Hemisphere, and (e) October mean in the polar Southern Hemisphere. Results are only shown for the eight CCMs that were run at least through 2050.

and Schoeberl, 2005]. Further analysis of CCMs is needed to determine the relative role of these two processes.

[37] Changes in ozone after 2050 primarily reflect changes in GHGs. In the three CCMs that ran beyond 2050, ozone continues to slowly increase except in the tropics (see discussion above). By the end of the 21st century the three CCMs predict that column ozone between 60°S and 60°N will be 1% to 4% above 1980 values.

4.2. Springtime Polar Ozone

[38] As in the midlatitudes, ozone in the polar regions in spring is also expected to respond to decreases in halogen loading and temperature changes through the 21st century. However, some of the processes affecting ozone recovery in the polar regions are different from those influencing extrapolar recovery. For example, GHG-induced cooling of the stratosphere reduces ozone destruction in extrapolar regions, but is likely to enhance it in the polar lower stratosphere where heterogeneous chemistry dominates, at least while halogen loading remains high (see section 3.2).

[39] In the polar regions we consider monthly mean total ozone anomalies of the area-weighted 60° to 90°N average in March in the Northern Hemisphere and 60° to 90°S average in October in the Southern Hemisphere. As just

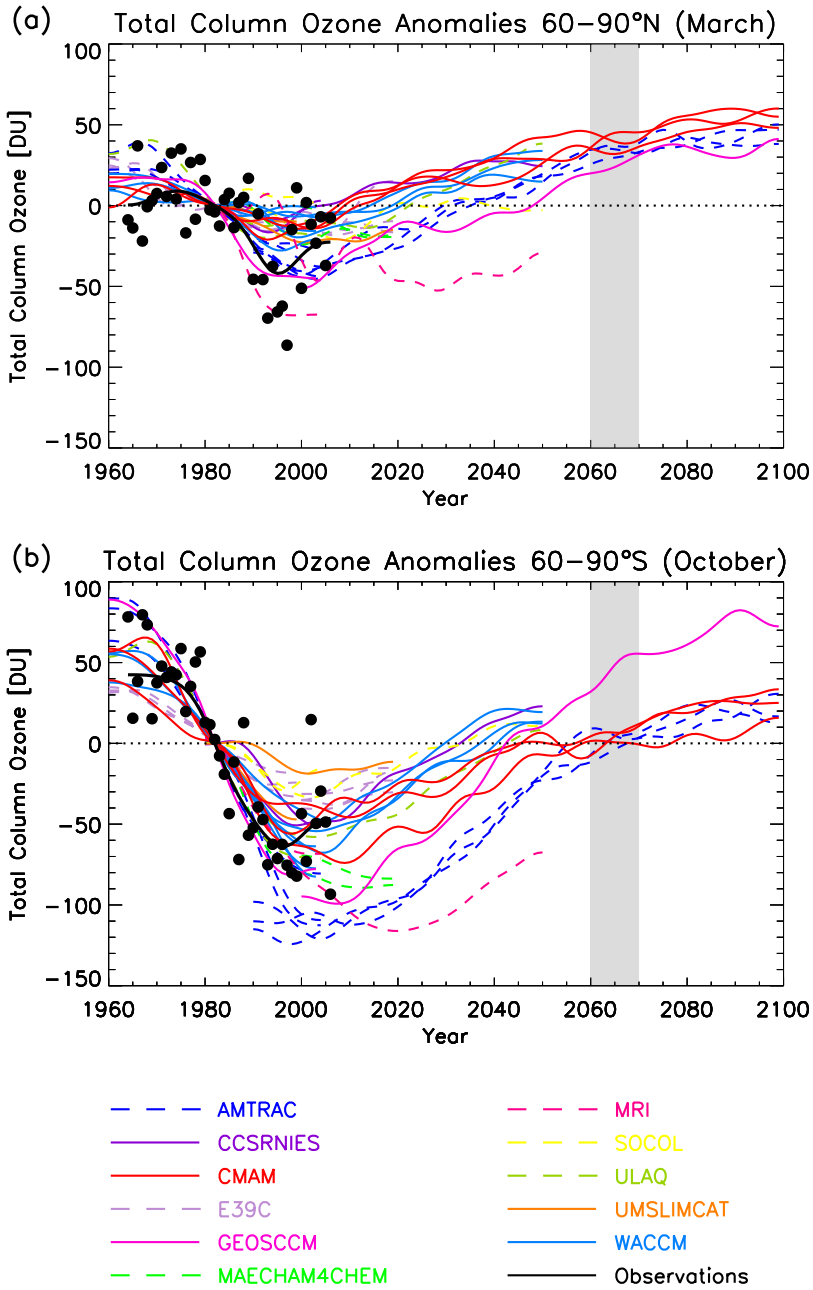

Figure 7. (a) March Arctic (60°N to 90°N) total column ozone anomalies from CCMs (colored lines) and the mean from four observational data sets (thick black line for smoothed curve and black dots for individual years). (b) As for Figure 7a, but October Antarctic (90°S to 60°S) total column ozone anomalies. Time series have been smoothed as in Figure 1 and anomalies have been calculated by subtracting the 1980–1984 mean from the smoothed time series. Light gray shading between 2060 and 2070 shows the period when stratospheric concentrations of halogens in the polar lower stratosphere are expected to return to their 1980 values.

1 month is shown and the interannual variability in polar regions is larger than in extrapolar regions, the total column ozone anomalies in polar regions are calculated by subtracting the 1980 to 1984 mean from the smoothed time series. Ideally, a longer period of pre-1980 years should be used to define the zero line [see, e.g., *Fioletov et al.*, 2002]. However, several model groups provided simulations that only started in 1980 and in order to apply a common method to all models and observations, this 5 year mean has been chosen. The absolute change in the total ozone anomalies shown in Figure 7, the agreement for an individual model with observations, and the date when a model returns to this "mean 1980" value are sensitive to the definition of the zero line, but the general conclusions drawn in this section hold. Following *Austin et al.* [2003] and *Bodeker et al.* [2005], we examine several additional ozone depletion indices: (1) The minimum daily total column ozone poleward of 60°N occurring during March–April (Arctic) and

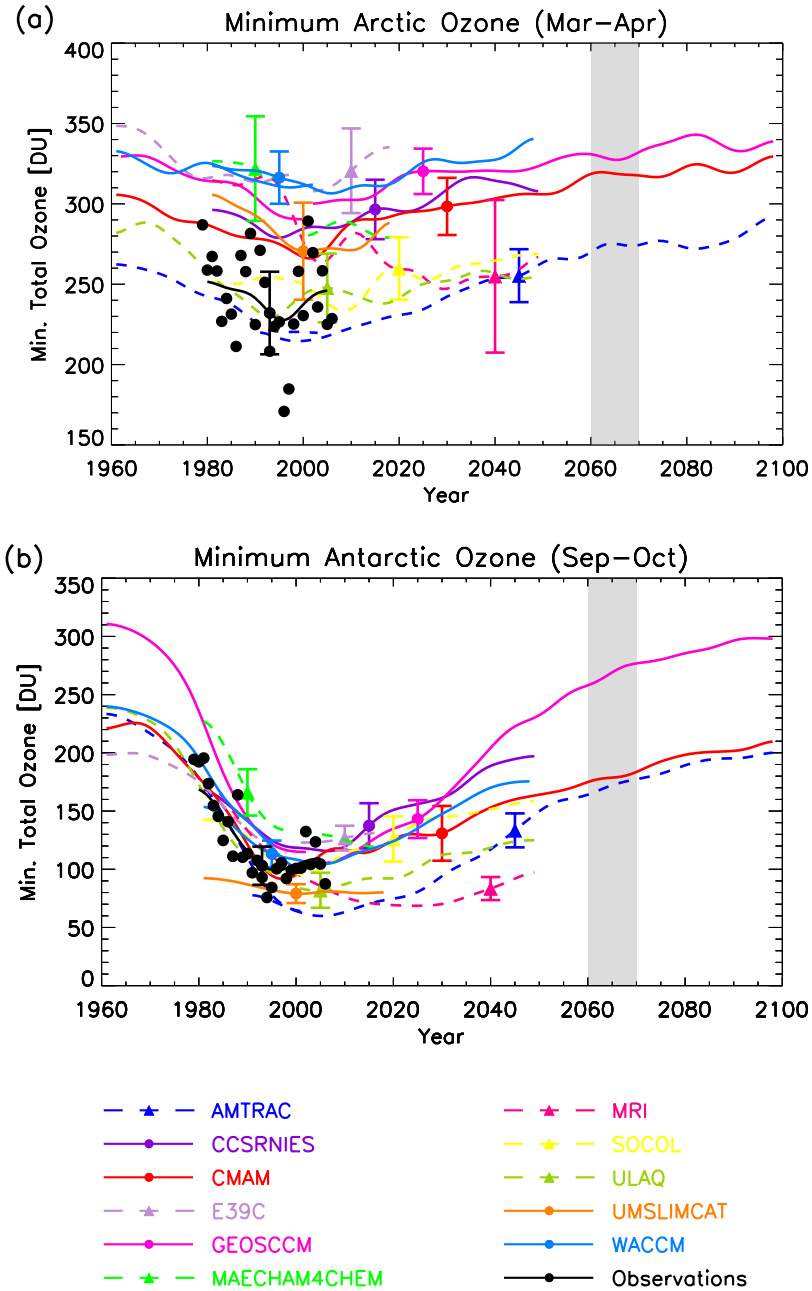

Figure 8. (a) Daily minimum Arctic total column ozone for March to April and (b) daily minimum Antarctic total column ozone for September to October for various transient CCM simulations. Model results are compared to values calculated from the NIWA assimilated total column ozone database [*Bodeker et al.*, 2005]. Time series have been smoothed as in Figure 1. Error bars denote plus or minus 1 standard deviation of the individual years from the smoothed curve. Light gray shading between 2060 and 2070 shows the period when stratospheric concentrations of halogens in the polar lower stratosphere are expected to return to their 1980 values.

poleward of 60°S occurring during September–October (Antarctic). (2) The ozone mass deficit calculated as the mean of daily values between September and October on the basis of a 220 DU threshold in the Antarctic [*Bodeker et al.*, 2005]. (3) The maximum daily Antarctic ozone hole area defined by the 220 DU contour that occurs between September and October in the Antarctic.

4.2.1. Antarctic

[40] In the Antarctic (60°–90°S) in spring, the general characteristics of ozone recovery are similar in all models and similar to the CCM predictions shown by *Austin et al.* [2003] and *WMO/UNEP* [2003]. Peak depletion occurs around 2000, with a broad minimum followed by a slow increase in ozone, see Figures 7, 8, and 9.

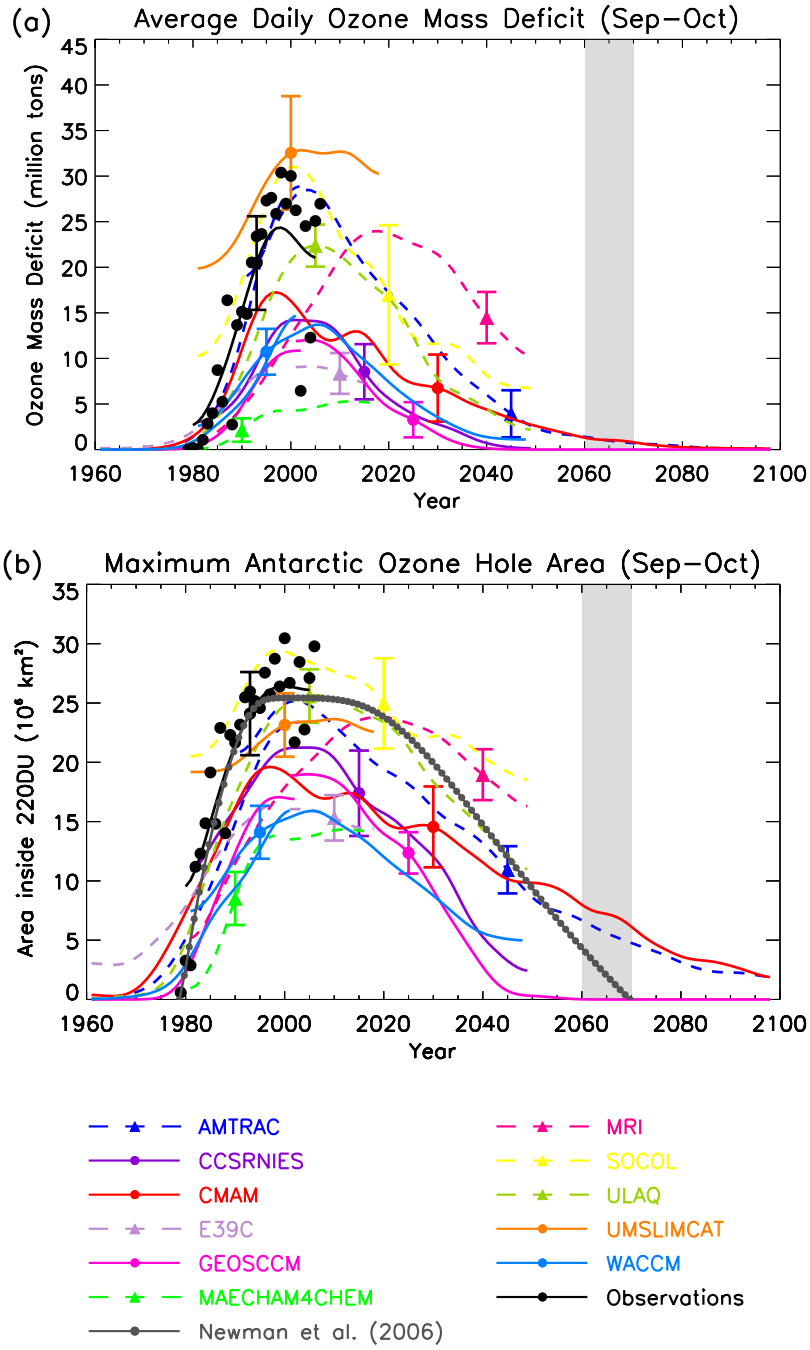

Figure 9. (a) Antarctic September to October average daily ozone mass deficit for each year from each CCM and (b) maximum Antarctic ozone hole area between September and October. Model results are compared to values calculated from the NIWA assimilated total column ozone database [*Bodeker et al.*, 2005]. Time series have been smoothed as in Figure 1. Error bars denote plus or minus 1 standard deviation of the individual years from the smoothed curve. Gray circles show the projection from *Newman et al.* [2006]. Light gray shading between 2060 and 2070 shows the period when stratospheric concentrations of halogens in the polar lower stratosphere are expected to return to their 1980 values.

[41] Although the general evolution is the same among the models, there are, as in extrapolar regions, quantitative differences among the CCMs, and between the CCMs and observations. In agreement with observations, between 1985 and 2006 all models simulate smaller column ozone values in October compared to their 1980–1984 mean (Figure 7). In AMTRAC a larger than observed decrease is simulated between 1995 and 2004, whereas other models show ozone anomalies only about half (E39C and SOCOL) or even less (UMSLIMCAT) than observed. There is quite a large spread in the pre-1980 ozone column anomalies. Part of this difference is due to the short period of 5 years

(1980–1984) used to calculate the anomalies. The Antarctic ozone hole at current EESC concentrations has low sensitivity to moderate decreases in EESC because nearly total loss of ozone occurs in the lowermost stratosphere inside the ozone hole in September and October and EESC concentrations often exceed those necessary to cause total loss. The unusually small ozone holes in some recent years in the observations (e.g., 2002 and 2004 [*WMO/UNEP*, 2007]) are related to a dynamically driven warmer Antarctic stratosphere in these years.

[42] The changes in ozone vary among the different ozone diagnostics between 2000 and 2020. The decrease in the magnitude of 60°–90°S October total column ozone anomalies and the increase in minimum Antarctic ozone are relatively slow, with values remaining almost constant between 2000 and 2010 in many models, whereas there is a relatively fast decrease in the ozone mass deficit. This behavior matches the differences in response between different Antarctic ozone hole indices seen in observations [*Bodeker et al.*, 2005]. The minimum in smoothed 60°–90°S October ozone anomalies varies between around −20 DU and −120 DU compared to observed values around −65 DU (Figure 7b). The smoothed minimum Antarctic ozone values in the CCMs vary between around 60 DU and 130 DU compared to observed values around 100 DU (Figure 8b), the peak smoothed ozone mass deficit varies between 5 and 33 million tons compared to observed values around 24 million tons (Figure 9a), while the peak smoothed maximum Antarctic ozone hole area varies from 15 to 30 million km^2 compared to 26 million km^2 in the observations. These variations highlight the deficiencies in some of the CCMs in the simulation of the present-day ozone hole, which are partly related to deficiencies in ability of the models to simulate Cl_y or to missing bromine chemistry. Note, however, that because both the ozone hole area and the ozone mass deficit are based on 220 DU thresholds, a general bias in the global mean total ozone fields, originating from latitude and altitude regions almost not affected by halogen chemistry, will generate a bias in these two diagnostics (most severe in MRI, MAECHAM4-CHEM, and E39C [see *Eyring et al.*, 2006, Figure 15c]) and the chemical signal cannot be properly evaluated. For example, whereas all CCMs underestimate the maximum ozone hole area since about 1990, SOCOL agrees best with observations around 2000. However, SOCOL is the model that underestimates Antarctic Cl_y most severely (Figure 1c) and has a large ozone mass deficit in 1980 (Figure 9a). This fact illustrates the complex interactions between dynamics and chemistry that result in the production of Antarctic ozone depletion and the need for more sophisticated metrics of model performance to understand how models generate ozone depletion. Possible techniques include the artificial passive ozone tracer technique or tracer-ozone relations [*Chipperfield et al.*, 2005; *Douglass et al.*, 2006; *Lemmen et al.*, 2006] or improved measures of the ozone mass deficit [*Huck et al.*, 2007].

[43] There is also a wide spread in predicted Antarctic ozone around and after 2050 when stratospheric halogen loading is expected to fall below 1980 values in the polar regions. For example, in 2050 anomalies in 60°–90°S ozone vary from around −20 to 20 DU and the minimum Antarctic ozone values vary between 125 and 230 DU (excluding MRI in both cases). For 2065 the values vary from 0 to 50 DU and 170 to 270 DU, respectively. In each model the dates when 60°–90°S October ozone anomalies and the three different Antarctic ozone indices return to their 1980 values are similar (within 5 to 10 years), but there is a large variation among the models in this date, varying between 2030 and 2070. Two out of the three CCMs that ran past 2050 predict that Antarctic ozone will be around 1980 values by the end of the century (2090–2100), but in one CCM (GEOSCCM) column ozone is much higher.

[44] As in extrapolar regions, there is an increase in middle and upper stratospheric ozone from the 1980s to the 2040s in all CCMs except MRI (Figure 6e). There are, however, very different changes in the lower stratosphere. Lower-stratospheric ozone is lower in the 2040s than in the 1980s in some CCMs (AMTRAC, CMAM, and MRI) and higher in others (CCSRNIES, GEOSCCM, SOCOL, and WACCM), which results in differences in the total ozone column anomalies in 2040–2050 (Figure 7).

[45] The difference in Cl_y among models appears to play a leading role in the differences in simulated ozone hole recovery discussed above. Comparison of Figure 1 with Figures 7 to 9 shows that, in general, models with smaller peak Cl_y and earlier return of Cl_y to 1980 values simulate smaller ozone depletion and an earlier ozone hole recovery: e.g., SOCOL and E39C have the smallest peak Cl_y and early Cl_y recovery, whereas AMTRAC has a larger peak and MRI a later peak Cl_y than observed, both showing later recovery. Also, UMSLIMCAT, which is close to observed Cl_y in terms of absolute amounts (Figure 1c), but which simulates only small changes in Cl_y and ESC because of incorrect initial conditions (Figures 1d and 1e) shows only small ozone trends. The close relationship between Cl_y, ESC, and minimum ozone is shown more clearly in Figure 10 (as discussed in section 3.1, ESC is not available for all models). The differences in the evolution of ozone among models are in general reflected in Cl_y and ESC. Also, for each model the evolution of minimum ozone is similar to that of Cl_y and ESC, and the date when minimum ozone returns to its 1980 value is generally similar to the dates when Cl_y and ESC return to their pre-1980 values (the horizontal lines in Figure 10 show the 1980 values of the fields). The correspondence between Cl_y or ESC and ozone in Figure 10 is, however, not exact. The minimum in the ozone time series is flatter than in Cl_y or ESC for some models (e.g., AMTRAC, CCSRNIES, and UMSLIMCAT), which is likely due to saturation effects (i.e., complete or near-complete ozone loss in regions where PSCs occur). There are variations in the timing of the return of Cl_y, ESC, and minimum ozone to their 1980 values. Some of these variations are due to issues with defining the "1980" values and smoothing of the ozone time series. Figure 10 also shows some anomalous features in individual CCMs discussed earlier, for example, the unrealistically low values of Cl_y but realistic ozone values in SOCOL, and the large values of ESC in 1980 and roughly constant ozone values from 1980 to 2020 in UMSLIMCAT.

[46] The above general agreement between Cl_y, ESC, 60°–90°S October total ozone anomalies and ozone hole indices, together with the analysis in section 3.1, provides some insight into possible biases in the CCMs ozone hole predictions. As discussed in section 3.1, most models have

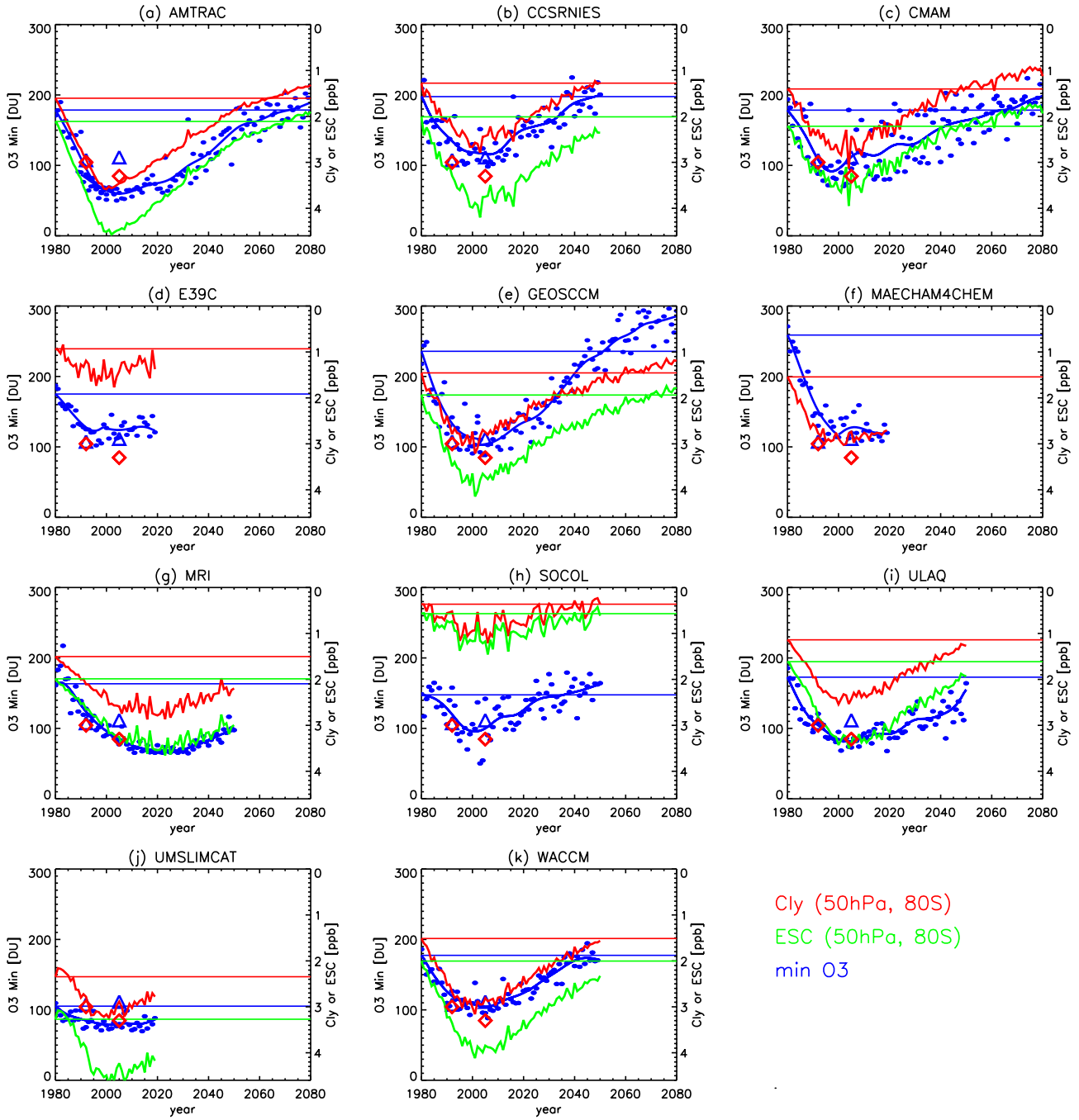

Figure 10. Daily minimum total column ozone (in DU) poleward of 60°S for September–October with total inorganic chlorine (Cl_y in ppb) and ESC (Cl_y + 60Br_y in ppb) at 50 hPa for October at 80°S superimposed. (a–k) Time series for the participating CCMs in alphabetical order. Triangles show observations for Cl_y and minimum ozone as in Figures 1c and 8b. For minimum ozone the blue circles show the individual years for each CCM and the solid lines show the smoothed curves as in Figure 8b. Horizontal lines indicate the 1980 values of the plotted quantities.

polar Cl_y that is too low (Figure 1), and models with lower peak Cl_y tend to simulate an earlier return of Cl_y to 1980 values. This combined with the above Cl_y – ozone relationship suggests that the recovery of ozone (around 2050) may occur too early in most models, with a large underestimate in those models that significantly underestimate the peak Cl_y (e.g., SOCOL). The one exception is AMTRAC which simulates a realistic peak Cl_y, and predicts the latest recover. We therefore might expect the date of ozone hole

recovery to occur even later, around 2060–2070 [see also *Austin and Wilson*, 2006].

[47] A recovery of Antarctic ozone after 2060 is consistent with the parametric modeling study of *Newman et al.* [2006]. This model uses estimates of EESC over Antarctica and analyzed Antarctic stratospheric temperatures to predict the evolution of the ozone hole. The gray circles in Figure 9b show the predicted ozone hole area from this parametric model: The ozone hole area is predicted to remain constant until around 2015, and then decrease to zero around 2068.

4.2.2. Arctic

[48] The evolution of Arctic springtime ozone is controlled by the combined effects of dynamical variability and halogen loading. Some CCMs show only little or no change in ozone over the Arctic, whereas others do respond to changes in halogen loading (Figures 7a and 8a). As in the other regions, Arctic ozone in spring is predicted to increase from 2000 to 2020. Using the smoothed minimum Arctic ozone column or 60°–90°N total ozone anomalies, where the smoothing reduces the large variability, the date of the minimum occurs between 1997 and 2015 in nearly all of the models. This time range is similar to that for Antarctica. Although the timing of the minimum ozone column is similar among the CCMs, there is a substantial variation in the magnitude of the minimum ozone column. In the smoothed time series the minimum varies from around 215 DU to over 300 DU, compared to around 230 DU in the observations (see Figure 8a). This again highlights some substantial biases in many of the models [see *Eyring et al.*, 2006].

[49] There is a wide range in the dates for simulated Arctic ozone to increase to 1980 values, with the date when smoothed 60°–90°N March ozone anomalies and minimum Arctic ozone return to 1980 values varying between around 2010 and 2045. However, all CCMs, except MRI, show an increase of column ozone to pre-1980 values before 2050 (Figure 7a) and increased stratospheric ozone in the 2040s compared to the 1980s (Figure 6d). None of the CCMs predict future large decreases in the Arctic column ozone.

[50] The return of ozone to pre-1980 values occurs before the modeled Cl_y decreases to 1980 concentrations (simulated Arctic Cl_y is very similar to the Antarctic Cl_y shown in Figure 1), and the projected evolution of Arctic ozone does not follow the evolution of halogens as closely as in the Antarctic; that is, the spread of the projected Arctic ozone is not strongly related to the spread in simulated Cl_y. Also, Arctic ozone increases to 1980 values before Antarctic ozone does. In some models the difference is only a few years, but in others the difference is over 25 years. This indicates that changes in other factors (e.g., temperature and transport) play a significant role in determining when Arctic ozone returns to pre-1980 values. *Austin and Wilson* [2006] reported that the earlier return to pre-1980 values in the Arctic in AMTRAC results from both an increased Brewer-Dobson circulation and reduced gas phase ozone depletion in a cooler stratosphere. However, it is unclear whether this is occurring in all models. In addition, the different treatment of chemistry and PSCs in the CCMs may contribute to the differences in the evolution of column ozone. For example, CCMs that do not include bromine chemistry underestimate ozone loss in particular in the Arctic [e.g., *Frieler et al.*, 2006]. Moreover, they will likely underestimate chemical ozone loss in their long-term projections of ozone throughout the 21st century, when stratospheric chlorine abundances decrease and bromine species become relatively more important [*Chipperfield and Pyle*, 1998; *WMO/UNEP*, 2007].

[51] The three CCMs that ran past 2050 (AMTRAC, CMAM, and GEOSCCM) all suggest that Arctic ozone in 2090 to 2100 will be substantially above 1980 values (10% to 20%), highlighting that by the end of the century factors other than ODSs will control stratospheric ozone in the Arctic.

5. Summary and Conclusions

[52] In this paper projections of stratospheric ozone in the 21st century from the current generation of coupled chemistry-climate models (CCMs) have been examined. This study extends the previous multimodel assessment [*Austin et al.*, 2003] by comparing only transient simulations with nearly identical forcings from a larger number of CCMs. For this purpose a set of consistent model forcings was defined as part of the CCM Validation Activity for SPARC (CCMVal; *Eyring et al.* [2005a, 2005b]). The forcings included natural and anthropogenic emissions based on existing scenarios, on atmospheric observations, and on the Kyoto and Montreal Protocols and their Amendments and Adjustments. The future simulations of the eleven CCMs participating in this study follow the Intergovernmental Panel on Climate Change (IPCC) Special Report on Emissions Scenarios (SRES) greenhouse gas (GHG) scenario A1B [*IPCC*, 2000] and the surface halogens are prescribed according to the Ab scenario of *WMO/UNEP* [2003]. Only a small number of the CCMs performed ensembles of simulations, and only one of those used different SSTs from different realizations of the same coupled general circulation model (GCM). However, with the time filtering used here, the ensemble spreads were generally much smaller than the intermodel differences. Thus the intermodel differences can be assessed from single simulations, without the use of ensembles.

[53] While the CCMs project similar long-term (1960–2100) evolution in ozone, there is a wide spread in the magnitude of past decreases in ozone and in future rates of ozone increases. However, there is sufficient agreement among the CCMs on the underlying causes of the ozone changes that general conclusions can be drawn and some confidence can be placed in their projections. In general, the future evolution of stratospheric ozone in the CCMs is mainly determined by decreases in halogen amounts and continued cooling of the global stratosphere due to increases in GHGs. The CCMs show large differences in peak Cl_y and timing of when future values have returned to modeled 1980 values, which is a major cause of the differences in simulated ozone recovery, in particular in the Antarctic. In contrast, the model-to-model agreement in projected temperature trends is good, and all CCMs predict continued, global mean cooling of the stratosphere over the next 5 decades, increasing from around 0.25 K/decade at 50 hPa to values of around 1 K/decade at 1 hPa. The magnitude of simulated changes in stratospheric water

vapor and NO_y suggests that they play only a minor role in simulated ozone recovery in the CCMs.

[54] All CCMs project extrapolar (60°S to 60°N) total column ozone to increase between 2000 and 2020, with most of the increase of 1% to 2.5% occurring after 2010. Over midlatitudes, the majority of the CCMs predict an increase of 1.5% to 3.5% between 2000 and 2020. As a result of ozone increases in the middle and upper stratosphere due to GHG-induced cooling, midlatitude, extrapolar, and global total ozone is projected to increase to 1980 values before lower-stratospheric halogen amounts decrease to 1980 values. Most CCMs predict northern midlatitude ozone returning to 1980 values before southern midlatitude ozone. After 2050 the ozone changes primarily reflect changes in GHGs and by 2100, ozone is projected to be above 1980 values.

[55] Simulated past ozone column changes over the tropics (25°S–25°N) are small compared to other regions but slightly overestimated compared to observations that show essentially no changes in this region over the period 1980–2004. Between 2000 and 2020 total column ozone increases of less than 2% are projected. The majority of the CCMs predict ozone columns that are similar or lower than 1980 values between 2040 and 2050 as a result of small decreases in tropical lower-stratospheric ozone. The negative trends in this region are likely related to increases in tropical upwelling. Another possible factor might be that increasing ozone in the upper stratosphere reduces the penetration of UV to the lower stratosphere reducing ozone production there (a reverse of the "self-healing" effect). Two out of three CCMs that were run to 2100 predict that tropical ozone is still below 1980 values by 2100.

[56] Maximum springtime ozone losses over the Antarctic (60°–90°S) occur between 2000 and 2010, and total column ozone is projected to increase by 5% to 10% between 2000 and 2020 because of decreases of stratospheric halogen concentrations. In the polar lower stratosphere in midwinter the CCMs simulate only small cooling trends in the first and second half of the 21st century, and large increases of the Antarctic ozone hole due to increased heterogeneous chemical ozone loss as a result of GHG-induced cooling in the lower stratosphere are not projected. Column ozone returns to 1980 values later than in midlatitudes because of the delay associated with transport of stratospheric air to polar regions. In most CCMs that time is around 2050, but as most models underestimate peak Cl_y, near 2000, ozone recovery may occur even later, between 2060 and 2070.

[57] Arctic (60°–90°N) springtime ozone is projected to increase by 0% to 10% between 2000 and 2020. While the large interannual variability in projected Arctic ozone obscures the date when the ozone turnaround due to decreasing halogens occurs, this is projected to occur before 2020. Increase in ozone does not follow halogen decreases as closely as in the Antarctic, reaching 1980 values before Arctic halogen amounts decrease to 1980 values and before the Antarctic. There is no indication of future large decreases in the Arctic column ozone in any of the model simulations and simulated temperature trends in the Arctic lower stratosphere in the 21st century are small. By 2100, Arctic ozone is projected to be substantially above 1980 values.

[58] Although most CCMs are able to reproduce important features of past global ozone depletion and a sophisticated model evaluation [*Eyring et al.*, 2006] has guided the assessment of the future predictions presented here, further analysis is required to assess how well all key processes that determine the evolution of stratospheric ozone are represented in the models. For example, further analysis is needed to understand the causes of the differences in future ozone projection in polar regions, and relative contribution of differences in dynamics and chemistry. This could include analysis of chemical ozone loss in the models, using artificial passive ozone tracers or tracer-ozone relations [*Chipperfield et al.*, 2005; *Douglass et al.*, 2006; *Lemmen et al.*, 2006] or improved measures of the ozone mass deficit [*Huck et al.*, 2007]. In addition, the frequency of occurrence of polar stratospheric clouds (PSCs) and the partitioning of the chemical families are important diagnostics to assess how well the chemistry is represented. Future research also needs to focus on the representation of the dynamics and variability in the CCMs. This includes the representation of vortex barriers and the frequency and timing of major midwinter stratospheric sudden warmings as a basic unit of stratospheric variability [*Charlton and Polvani*, 2007]. If the models have problems to simulate correctly the size of the vortex, the breakup date of the vortex, or the strength of the transport barrier at the edge of the polar vortex, this will have implications on quantities like total column ozone anomalies poleward of 60° [e.g., *WMO/UNEP*, 2007].

[59] In addition to the above, several other considerations suggest that the ozone projections must be used with caution. First, there are uncertainties that are directly related to parameterized processes in the CCMs themselves. For example, sub-grid-scale processes like gravity wave propagation and breaking or convection are parameterized in a way that is tuned to past and present conditions and assumed to be the same in the future. There are also uncertainties in the simulated future chemistry-climate feedbacks [*WMO/UNEP*, 2007, chapter 5]. Changes in the generation and propagation of planetary-scale waves may affect stratospheric ozone [e.g., *Stolarski et al.*, 2006a]. These changes and those in the sub-grid-scale momentum deposition presumably give rise to the projected increase in the Brewer-Dobson circulation [*Butchart et al.*, 2006; *Rind et al.*, 1998; *Sigmond et al.*, 2004]. While the increase in the Brewer-Dobson circulation appears to be a robust feature of climate model simulations, the rate of change of the circulation varies substantially from one model to the next. Finally, the projected ozone in 2100 is sensitive to future levels of GHGs. Different scenarios of future emissions of GHGs will, in addition to radiative effects, result in a different chemical composition of the stratosphere through the production of radicals which catalytically destroy ozone [e.g., *Chipperfield and Feng*, 2003]. In the simulations presented in this intercomparison, only a single GHG scenario has been used.

[60] **Acknowledgments.** Coordination of this study was supported by the Chemistry-Climate Model Validation activity (CCMVal) for World Climate Research Programme (WCRP)'s Stratospheric Processes and their Role in Climate (SPARC) project. We thank the British Atmospheric Data Centre, the SPARC data center, and the U.K. Met Office for providing the facilities for central data archives. Special thanks go to David Lary for

providing analysis of spaceborne measurements of inorganic chlorine and to Vitali Fioletov for providing observational data sets of monthly average zonal total ozone from ground-based measurements and merged satellite data. We also greatly appreciate comments on the manuscript by three anonymous reviewers. DWW's research was supported by a NASA grant. JA's research was supported by the Visiting Scientist Program at the NOAA Geophysical Fluid Dynamics Laboratory, administered by the University Corporation for Atmospheric Research. CCSRNIES' and MRI's research was supported by the Global Environmental Research Fund (GERF) of the Ministry of the Environment (MOE) of Japan (A-1). CMAM is supported by CFCAS and NSERC. The Leeds work was supported by the U.K. Natural Environment Research Council (NERC). Computational resources for running the GEOSCCM were provided by NASA's high-performance computing project. The SOCOL group was supported by the Swiss Federal Institute of Technology and in part by the Swiss National Science Foundation (grant SCOPES IB7320-110884). The European groups acknowledge support of the SCOUT-O3 Integrated Project which is funded by the European Commission.

References

Akiyoshi, H., T. Sugita, H. Kanzawa, and N. Kawamoto (2004), Ozone perturbations in the Arctic summer lower stratosphere as a reflection of NO_x chemistry and planetary scale wave activity, *J. Geophys. Res.*, *109*, D03304, doi:10.1029/2003JD003632.

Anderson, J., J. M. Russell III, S. Solomon, and L. E. Deaver (2000), Halogen Occultation Experiment confirmation of stratospheric chlorine decreases in accordance with the Montreal Protocol, *J. Geophys. Res.*, *105*, 4483–4490.

Austin, J., and F. Li (2006), On the relationship between the strength of the Brewer-Dobson circulation and the age of stratospheric air, *Geophys. Res. Lett.*, *33*, L17807, doi:10.1029/2006GL026867.

Austin, J., and R. J. Wilson (2006), Ensemble simulations of the decline and recovery of stratospheric ozone, *J. Geophys. Res.*, *111*, D16314, doi:10.1029/2005JD006907.

Austin, J., et al. (2003), Uncertainties and assessments of chemistry-climate models of the stratosphere, *Atmos. Chem. Phys.*, *3*, 1–27.

Austin, J., R. J. Wilson, F. Li, and H. Vömel (2006), Evolution of water vapor concentrations and stratospheric age of air in coupled chemistry-climate model simulations, *J. Atmos. Sci.*, *64*(3), 905–921.

Beagley, S. R., J. de Grandpré, J. N. Koshyk, N. A. McFarlane, and T. G. Shepherd (1997), Radiative-dynamical climatology of the first-generation Canadian middle atmosphere model, *Atmos. Ocean*, *35*, 293–331.

Bodeker, G. E., H. Shiona, and H. Eskes (2005), Indicators of Antarctic ozone depletion, *Atmos. Chem. Phys.*, *5*, 2603–2615.

Butchart, N., and A. A. Scaife (2001), Removal of chlorofluorocarbons by increased mass exchange between the stratosphere and troposphere in a changing climate, *Nature*, *410*, 799–802.

Butchart, N., et al. (2006), Simulations of anthropogenic change in the strength of the Brewer-Dobson circulation, *Clim. Dyn.*, *27*, 727–741.

Charlton, A. J., and L. M. Polvani (2007), A new look at stratospheric sudden warmings. Part I: Climatology and modeling benchmarks, *J. Clim.*, *20*, 449–469, doi:10.1175/JCLI3996.1.

Chipperfield, M. P., and W. Feng (2003), Comment on: "Stratospheric ozone depletion at northern mid-latitudes in the 21st century: The importance of future concentrations of greenhouse gases nitrous oxide and methane", *Geophys. Res. Lett.*, *30*(7), 1389, doi:10.1029/2002GL016353.

Chipperfield, M. P., and J. A. Pyle (1998), Model sensitivity studies of Arctic ozone depletion, *J. Geophys. Res.*, *103*, 28,389–28,403.

Chipperfield, M. P., W. Feng, and M. Rex (2005), Arctic ozone loss and climate sensitivity: Updated three-dimensional model study, *Geophys. Res. Lett.*, *32*, L11813, doi:10.1029/2005GL022674.

Cordero, E. C., and P. M. de Forster (2006), Stratospheric variability and trends in IPCC model simulations, *Atmos. Chem. Phys.*, *6*, 7657–7695.

Dameris, M., et al. (2005), Long-term changes and variability in a transient simulation with a chemistry-climate model employing realistic forcings, *Atmos. Chem. Phys.*, *5*, 2121–2145.

Dameris, M., S. Matthes, R. Deckert, V. Grewe, and M. Ponater (2006), Solar cycle effect delays onset of ozone recovery, *Geophys. Res. Lett.*, *33*, L03806, doi:10.1029/2005GL024741.

de Grandpré, J., S. R. Beagley, V. I. Fomichev, E. Griffioen, J. C. McConnell, A. S. Medvedev, and T. G. Shepherd (2000), Ozone climatology using interactive chemistry: Results from the Canadian middle atmosphere model, *J. Geophys. Res.*, *105*, 26,475–26,492.

Douglass, A. R., M. R. Schoeberl, R. S. Stolarski, J. W. Waters, J. M. Russell III, and A. E. Roche (1995), Interhemispheric differences in springtime production of HCl and $ClONO_2$ in the polar vortices, *J. Geophys. Res.*, *100*, 13,967–13,978.

Douglass, A., R. Stolarski, S. Strahan, and B. Polansky (2006), Sensitivity of Arctic ozone loss to polar stratospheric cloud volume and chlorine and bromine loading in a chemistry and transport model, *Geophys. Res. Lett.*, *33*, L17809, doi:10.1029/2006GL026492.

Dvortsov, V. L., and S. Solomon (2001), Response of the stratospheric temperatures and ozone to past and future increases in stratospheric humidity, *J. Geophys. Res.*, *106*, 7505–7514.

Egorova, T., E. Rozanov, V. Zubov, E. Manzini, W. Schmutz, and T. Peter (2005), Chemistry-climate model SOCOL: A validation of the present-day climatology, *Atmos. Chem. Phys.*, *5*, 1557–1576.

Eyring, V., et al. (2005a), A strategy for process-oriented validation of coupled chemistry-climate models, *Bull. Am. Meteorol. Soc.*, *86*, 1117–1133.

Eyring, V., D. E. Kinnison, and T. G. Shepherd (2005b), Overview of planned coupled chemistry-climate simulations to support upcoming ozone and climate assessments, *SPARC Newsl.*, *25*, 11–17.

Eyring, V., et al. (2006), Assessment of temperature, trace species, and ozone in chemistry-climate model simulations of the recent past, *J. Geophys. Res.*, *111*, D22308, doi:10.1029/2006JD007327.

Fioletov, V. E., G. E. Bodeker, A. J. Miller, R. D. McPeters, and R. Stolarski (2002), Global ozone and zonal total ozone variations estimated from ground-based and satellite measurements: 1964–2000, *J. Geophys. Res.*, *107*(D22), 4647, doi:10.1029/2001JD001350.

Fomichev, V. I., A. I. Jonsson, J. de Grandpré, S. R. Beagley, C. McLandress, K. Semeniuk, and T. G. Shepherd (2007), Response of the middle atmosphere to CO_2 doubling: Results from the Canadian middle atmosphere model, *J. Clim.*, *20*, 1121–1144.

Frieler, K., M. Rex, R. J. Salawitch, T. Canty, M. Streibel, R. M. Stimpfle, K. Pfeilsticker, M. Dorf, D. K. Weisenstein, and S. Godin-Beekmann (2006), Toward a better quantitative understanding of polar stratospheric ozone loss, *Geophys. Res. Lett.*, *33*,, L10812, doi:10.1029/2005GL025466.

Froidevaux, L., et al. (2006), Temporal decrease in upper atmospheric chlorine, *Geophys. Res. Lett.*, *33*, L23812, doi:10.1029/2006GL027600.

Garcia, R. R., D. R. Marsh, D. E. Kinnison, B. A. Boville, and F. Sassi (2007), Simulation of secular trends in the middle atmosphere, 1950–2003, *J. Geophys. Res.*, *112*, D09301, doi:10.1029/2006JD007485.

Gates, W. L., et al. (1999), An overview of the results of the atmospheric model intercomparison projects (AMIP), *Bull. Am. Meteorol. Soc.*, *80*, 29–56.

Giorgetta, M. A., and L. Bengtsson (1999), The potential role of the quasi-biennial oscillation in the stratosphere-troposphere exchange as found in water vapor in general circulation model experiments, *J. Geophys. Res.*, *104*, 6003–6020.

Haigh, J. D., and J. A. Pyle (1982), Ozone perturbation experiments in a two-dimensional circulation model, *Q. J. R. Meteorol. Soc.*, *108*, 551–574.

Huck, P. E., A. J. McDonald, G. E. Bodeker, and H. Struthers (2005), Interannual variability in Antarctic ozone depletion controlled by planetary waves and polar temperatures, *Geophys. Res. Lett.*, *32*, L13819, doi:10.1029/2005GL022943.

Huck, P. E., S. Tilmes, G. E. Bodeker, W. J. Randel, A. J. McDonald, and H. Nakajima (2007), An improved measure of ozone depletion in the Antarctic stratosphere, *J. Geophys. Res.*, *112*, D11104, doi:10.1029/2006JD007860.

Intergovernmental Panel on Climate Change (IPCC) (2000), *Special Report on Emissions Scenarios*, edited by N. Nakicenovic et al., 599 pp., Cambridge Univ. Press, New York.

Intergovernmental Panel on Climate Change and Technology and Economic Assessment Panel (IPCC/TEAP) (2005), *Special Report on Safeguarding the Ozone Layer and the Global Climate System: Issues Related to Hydrofluorocarbons and Perfluorocarbons*, Cambridge Univ. Press, New York.

Johns, T. C., et al. (2006), The new Hadley Centre climate model HadGEM1: Evaluation of coupled simulations, *J. Clim.*, *19*, 1327–1353.

Jonsson, A. I., J. de Grandpré, V. I. Fomichev, J. C. McConnell, and S. R. Beagley (2004), Doubled CO_2-induced cooling in the middle atmosphere: Photochemical analysis of the ozone radiative feedback, *J. Geophys. Res.*, *109*, D24103, doi:10.1029/2004JD005093.

Kirk-Davidoff, D. B., E. J. Hintsa, J. G. Anderson, and D. W. Keith (1999), The effect of climate change on ozone depletion through changes in stratospheric water vapour, *Nature*, *40*, 399–401.

Kurokawa, J., H. Akiyoshi, T. Nagashima, H. Masunaga, T. Nakajima, M. Takahashi, and H. Nakane (2005), Effects of atmospheric sphericity on stratospheric chemistry and dynamics over Antarctica, *J. Geophys. Res.*, *110*, D21305, doi:10.1029/2005JD005798.

Lean, J. L. (2000), Evolution of the Sun's spectral irradiance since the maunder minimum, *Geophys. Res. Lett.*, *27*, 2425–2428.

Lean, J. L., G. J. Rottman, H. L. Kyle, T. N. Woods, J. R. Hickey, and L. C. Puga (1997), Detection and parameterization of variations in solar mid- and near-ultraviolet radiation (200 to 400 nm), *J. Geophys. Res.*, *102*, 29,939–29,956.

Lemmen, C., M. Dameris, R. Müller, and M. Riese (2006), Chemical ozone loss in a chemistry-climate model from 1960 to 1999, *Geophys. Res. Lett.*, *33*, L15820, doi:10.1029/2006GL026939.

Manzini, E., B. Steil, C. Brühl, M. A. Giorgetta, and K. Krüger (2003), A new interactive chemistry climate model: 2. Sensitivity of the middle atmosphere to ozone depletion and increase in greenhouse gases and implications for recent stratospheric cooling, *J. Geophys. Res.*, *108*(D14), 4429, doi:10.1029/2002JD002977.

Miller, A. J., et al. (2002), A cohesive total ozone data set from SBUV(/2) satellite system, *J. Geophys. Res.*, *107*(D23), 4701, doi:10.1029/2001JD000853.

Montzka, S. A., J. H. Butler, B. D. Hall, D. J. Mondeel, and J. W. Elkins (2003), A decline in tropospheric bromine, *Geophys. Res. Lett.*, *30*(15), 1826, doi:10.1029/2003GL017745.

Newman, P. A., S. R. Kawa, and E. R. Nash (2004), On the size of the Antarctic ozone hole, *Geophys. Res. Lett.*, *31*, L21104, doi:10.1029/2004GL020596.

Newman, P. A., E. R. Nash, S. R. Kawa, S. A. Montzka, and S. M. Schauffler (2006), When will the Antarctic ozone hole recover?, *Geophys. Res. Lett.*, *33*, L12814, doi:10.1029/2005GL025232.

Pitari, G., E. Mancini, V. Rizi, and D. Shindell (2002), Impact of future climate and emission changes on stratospheric aerosols and ozone, *J. Atmos. Sci.*, *59*, 414–440.

Randeniya, L. K., P. F. Vohralik, and I. C. Plumb (2002), Stratospheric ozone depletion at northern mid latitudes in the 21st century: The importance of future concentrations of greenhouse gases nitrous oxide and methane, *Geophys. Res. Lett.*, *29*(4), 1051, doi:10.1029/2001GL014295.

Rayner, N. A., D. E. Parker, E. B. Horton, C. K. Folland, L. V. Alexander, D. P. Rowell, E. C. Kent, and A. Kaplan (2003), Global analyses of sea surface temperature, sea ice, and night marine air temperature since the late nineteenth century, *J. Geophys. Res.*, *108*(D14), 4407, doi:10.1029/2002JD002670.

Rex, M., R. J. Salawitch, P. von der Gathen, N. R. P. Harris, M. Chipperfield, and B. Naujokat (2004), Arctic ozone loss and climate change, *Geophys. Res. Lett.*, *31*, L04116, doi:10.1029/2003GL018844.

Rind, D., D. Shindell, P. Lonergan, and N. K. Balachandran (1998), Climate change and the middle atmosphere. Part III: The doubled CO_2 climate revisited, *J. Clim.*, *11*, 876–894.

Rosenfield, J. E., and A. R. Douglass (1998), Doubled CO_2 effects on NO_y in a coupled 2D model, *Geophys. Res. Lett.*, *25*, 4381–4384.

Rosenfield, J. E., and M. R. Schoeberl (2005), Recovery of the tropical lower stratospheric ozone layer, *Geophys. Res. Lett.*, *32*, L21806, doi:10.1029/2005GL023626.

Rosenfield, J. E., A. R. Douglass, and D. B. Considine (2002), The impact of increasing carbon dioxide on ozone recovery, *J. Geophys. Res.*, *107*(D6), 4049, doi:10.1029/2001JD000824.

Rozanov, E., M. Schraner, C. Schnadt, T. Egorova, M. Wild, A. Ohmura, V. Zubov, W. Schmutz, and T. Peter (2005), Assessment of the ozone and temperature variability during 1979–1993 with the chemistry-climate model SOCOL, *Adv. Space. Res.*, *35*(8), 1375–1384.

Santee, M. L., L. Froidevaux, G. L. Manney, W. G. Read, J. W. Waters, M. P. Chipperfield, A. E. Roche, J. B. Kumer, J. L. Mergenthaler, and J. M. Russell III (1996), Chlorine deactivation in the lower stratospheric polar regions during late winter: Results from UARS, *J. Geophys. Res.*, *101*, 18,835–18,860.

Schmidt, H., G. Brasseur, M. Charron, E. Manzini, M. A. Giorgetta, V. Fomichev, D. Kinnison, D. Marsh, and S. Walters (2006), The HAMMONIA chemistry climate model: Sensitivity of the mesopause region to the 11-year solar cycle and CO_2 doubling, *J. Clim.*, *19*, 3903–3931.

Shibata, K., and M. Deushi (2005), Partitioning between resolved wave forcing and unresolved gravity wave forcing to the quasi-biennial oscillation as revealed with a coupled chemistry-climate model, *Geophys. Res. Lett.*, *32*, L12820, doi:10.1029/2005GL022885.

Shibata, K., M. Deushi, T. T. Sekiyama, and H. Yoshimura (2005), Development of an MRI chemical transport model for the study of stratospheric chemistry, *Pap. Meteorol. Geophys.*, *55*, 75–119.

Shindell, D. T. (2001), Climate and ozone response to increased stratospheric water vapor, *Geophys. Res. Lett.*, *28*, 1551–1554.

Shiogama, H., M. Watanabe, M. Kimoto, and T. Nozawa (2005), Anthropogenic and natural forcing impacts on ENSO-like decadal variability during the second half of the 20th century, *Geophys. Res. Lett.*, *32*, L21714, doi:10.1029/2005GL023871.

Sigmond, M., P. C. Siegmund, E. Manzini, and H. Kelder (2004), A simulation of the separate climate effects of middle atmospheric and tropospheric CO_2 doubling, *J. Clim.*, *17*, 2352–2367.

Steil, B., C. Brühl, E. Manzini, P. J. Crutzen, J. Lelieveld, P. J. Rasch, E. Roeckner, and K. Krüger (2003), A new interactive chemistry climate model: 1. Present day climatology and interannual variability of the middle atmosphere using the model and 9 years of HALOE/UARS data, *J. Geophys. Res.*, *108*(D9), 4290, doi:10.1029/2002JD002971.

Stenke, A., and V. Grewe (2005), Simulation of stratospheric water vapor trends: Impact on stratospheric ozone chemistry, *Atmos. Chem. Phys.*, *5*, 1257–1272.

Stolarski, R. S., and S. Frith (2006), Search for evidence of trend slowdown in the long-term TOMS/SBUV total ozone data record: The importance of instrument drift uncertainty, *Atmos. Chem. Phys.*, *6*, 4057–4065.

Stolarski, R. S., A. R. Douglass, S. Steenrod, and S. Pawson (2006a), Trends in stratospheric ozone: Lessons learned from a 3D chemical transport model, *J. Atmos. Sci.*, *63*, 1028–1041.

Stolarski, R. S., A. R. Douglass, M. Gupta, P. A. Newman, S. Pawson, M. R. Schoeberl, and J. E. Nielsen (2006b), An ozone increase in the Antarctic summer stratosphere: A dynamical response to the ozone hole, *Geophys. Res. Lett.*, *33*, L21805, doi:10.1029/2006GL026820.

Tabazadeh, A., M. L. Santee, M. Y. Danilin, H. C. Pumphrey, P. A. Newman, P. J. Hamill, and J. L. Mergenthaler (2000), Quantifying denitrification and its effect on ozone recovery, *Science*, *288*, 1407–1411.

Taylor, K. E., D. Williamson, and F. Zwiers (2000), The sea surface temperature and sea-ice concentration boundary concentrations for AMIP II simulations, *PMCDI Report 60*, Prog. for Clim. Model Diagnosis and Intercomparison, Lawrence Livermore Natl. Lab., Livermore, Calif.

Tian, W., and M. P. Chipperfield (2005), A new coupled chemistry-climate model for the stratosphere: The importance of coupling for future O3-climate predictions, *Q. J. R. Meteorol. Soc.*, *131*, 281–304.

Tian, W., M. P. Chipperfield, L. J. Gray, and J. M. Zawodny (2006), Quasi-biennial oscillation and tracer distributions in a coupled chemistry-climate model, *J. Geophys. Res.*, *111*, D20301, doi:10.1029/2005JD006871.

Tilmes, S., R. Müller, J.-U. Grooß, and J. M. Russell III (2004), Ozone loss and chlorine activation in the Arctic winters 1991–2003 derived with the tracer-tracer correlations, *Atmos. Chem. Phys.*, *4*(8), 2181–2213.

Waugh, D. W., D. B. Considine, and E. L. Fleming (2001), Is upper stratospheric chlorine decreasing as expected?, *Geophys. Res. Lett.*, *28*, 1187–1190.

World Meteorological Organization/United Nations Environment Programme (WMO/UNEP) (2003), Scientific Assessment of Ozone Depletion: 2002, *Rep. 47*, World Meteorol. Org., Global Ozone Res. and Monit. Proj., Geneva, Switzerland.

World Meteorological Organization/United Nations Environment Programme (WMO/UNEP) (2007), Scientific Assessment of Ozone Depletion: 2006, *Rep. 50*, World Meteorol. Org., Global Ozone Res. and Monit. Proj., Geneva, Switzerland.

Yukimoto, S., A. Noda, T. Uchiyama, S. Kusunoki, and A. Kitoh (2005), Climate changes of the twentieth through twenty-first centuries simulated by the MRI-CGCM2.3., *Pap. Meteorol. Geophys.*, *56*, 9–24.

H. Akiyoshi, T. Nagashima, and M. Yoshiki, National Institute for Environmental Studies, Tsukuba 305-8506, Japan.

J. Austin, Geophysical Fluid Dynamics Laboratory, NOAA, Princeton, NJ 08542-0308, USA.

S. R. Beagley and K. Semeniuk, Department of Earth and Space Science and Engineering, York University, Toronto, Canada, ON M3J 1P3.

G. E. Bodeker, National Institute of Water and Atmospheric Research, Lauder, New Zealand.

P. Braesicke, Centre for Atmospheric Science, Cambridge University, Cambridge, UK.

N. Butchart, Climate Research Division, Met Office, Exeter EX1 3PB, UK.

B. A. Boville, R. R. Garcia, A. Gettelman, D. E. Kinnison, and D. R. Marsh, National Center for Atmospheric Research, Boulder, CO 80307, USA.

C. Brühl and B. Steil, Max Planck Institut für Chemie, D-55128 Mainz, Germany.

M. P. Chipperfield and W. Tian, Institute for Atmospheric Science, University of Leeds, Leeds, LS2 9JT, UK.

E. Cordero, Department of Meteorology, San Jose State University, San Jose, CA 95192, USA.

M. Dameris, R. Deckert, V. Eyring, and S. Matthes, Institut für Physik der Atmosphäre, Deutsches Zentrum für Luft- und Raumfahrt, Oberpfaffenhofen, D-82234 Wessling, Germany. (veronika.eyring@dlr.de)

M. Deushi and K. Shibata, Meteorological Research Institute, Tsukuba 305-0052, Japan.

S. M. Frith and J. E. Nielsen, Science Systems and Applications, Incorporated, Lanham, MD 20706, USA.

M. A. Giorgetta, Max Planck Institut für Meteorologie, D-20146 Hamburg, Germany.

E. Mancini and G. Pitari, Dipartimento di Fisica, Università L'Aquila, Via Vetoio, I-67010 L'Aquila, Italy.

E. Manzini, Istituto Nazionale di Geofisica e Vulcanologia and Centro Euro-Mediterraneo per i Cambiamenti Climatici, I-40128 Bologna, Italy.

P. A. Newman, S. Pawson, and R. S. Stolarski, NASA Goddard Space Flight Center, Greenbelt, MD 20771, USA.

D. A. Plummer, Ouranos Consortium, 550 rue Sherbrooke Ouest, 19e étage, Montréal, QC, Canada H3A 1B9.

E. Rozanov, Physical-Meteorological Observatory/World Radiation Center, CH-7260 Davos, Switzerland.

M. Schraner, Institute for Atmospheric and Climate Science, ETH Zurich, CH-8092 Zurich, Switzerland.

J. F. Scinocca, Canadian Centre for Climate Modelling and Analysis, Meteorological Service of Canada, University of Victoria, Victoria BC V8W 2Y2, Canada.

T. G. Shepherd, Department of Physics, University of Toronto, Toronto, ON, Canada M5S 1A7.

D. W. Waugh, Department of Earth and Planetary Sciences, Johns Hopkins University, Baltimore, MD 21218, USA.